The approach to Equilibration in Closed Quantum Systems

Dissertation

zur Erlangung des Grades eines Doktors der
Naturwissenschaften (Dr. rer. nat.)

dem Fachbereich Physik der Universität Osnabrück vorgelegt
von

Hendrik Niemeyer, M. Sc.

Osnabrück, im November 2013

Abstract

The question whether and how closed quantum systems equilibrate is still debated today. In this thesis a generic spin system is analysed and criteria to classify unique equilibration dynamics are developed. Furthermore, the eigenstate thermalization hypothesis is investigated as a possible cause for the unique equilibrium. For both problems novel numerical methods for solving the time-dependent Schroedinger equation based on series expansions and typicality are developed. Furthermore, the problem of markovian dynamics on the level of single measurements is discussed.

Contents

1. Introduction

When a cup of hot coffee is prepared and left alone in a room for quite some time the coffee will have emitted heat to the air in the room and both systems “air” and “coffee” will have reached the same temperature (the larger room a littler higher than before, the cup of coffee unfortunately a lot lower than before). This effect which is a description of thermalization in physics laymen terms is widely observed in our macroscopic world. Thermalization is universal in the sense that it happens to every combination of macroscopic systems which differ in a certain thermodynamic variable like temperature, pressure, etc. with the equilibrium not depending of the microstate of the system at time of preparation. Therefore, the scenario with the hot coffee and cold air could be prepared again and again with the same temperature difference but more or less uncontrolled otherwisely and the measured decay of temperature into equilibrium would still be the same.

On a macroscopic, phenomenological level these processes are well understood and can be found in every standard textbook on thermodynamics. Essentially, thermodynamic variables evolve following a diffusion process, which means that the relaxation towards equilibrium of the considered thermodynamic variable is Markovian and autonomous (there are no relevant hidden variables) in the sense that regardless of the difference in this variable between the considered systems at time of preparation the relaxation dynamics all have the same relaxation constant and are free of memory effects. While from a phenomenological point of view it is clear what to expect in such a scenario its microscopical foundations are still a topic of research [1, 2, 3]: From a microscopical perspective every system regardless of its size is mechanical. Therefore, the above mentioned thermalization process must be somehow included in the physical description of quantum mechanics since all systems can be ultimately described as a closed quantum system. But the fundamental equation governing quantum mechanics, the time-dependent Schroedinger equation, is linear and does not feature any attractive fixed

point. Therefore, bridging the gap between quantum mechanics and thermodynamics is still a subject of research today although both disciplines of physics have been subject to research and discussion for a long time. Consequently, already in the early formulations of quantum mechanics [4, 5, 6, 7, 8] the question about the relationship between quantum mechanics and thermodynamics arose. A central point in the discussion is the reconciliation of unitary quantum dynamics (featuring no fixed point) with the equilibrating, rate equation-type dynamics of non-equilibrium thermodynamics (featuring a fixed point). In this debate various concepts have been introduced such as "typicality" [5, 9, 10, 2, 11, 12], "pure state quantum statistical mechanics" [13, 14, 15] "eigenstate thermalization hypothesis" [5, 16, 17, 18, 19], "thermal environment coupling" [20, 21, 22], and many more. Recently, experiments in an optical lattice with ultra-cold atoms have been performed to study the relaxation dynamics in an interacting many-body system [23]. Also the thermalization dynamics itself, beyond the mere existence of equilibrium, has gained attention: Fokker-Planck equations for some closed finite quantum systems have been suggested [24, 25, 26, 27].

In this thesis the above mentioned, archetypical example of non-equilibrium thermodynamics (a hot and cold body exchanging heat and thermalizing) is discussed on a closed quantum system which shall stand as a model for this scenario on a microscopic level. It is checked whether its dynamics according to the standard time-dependent Schroedinger equation show signature signs of thermodynamic behavior in the sense as mentioned above. The eigenstate thermalization hypothesis is discussed for this quantum system as a possible factor in its unique equilibration process and a novel method for analyzing the eigenstate thermalization hypothesis is developed for Hamiltonians which are too large to be diagonalized in reasonable time utilizing numerical methods used in solving systems of ordinary differential equations.

This thesis is organized as follows: In chapter 2 the fundamental concepts of equilibration and thermalization are briefly introduced and discussed and the "axioms of unique equilibration" derived from macroscopic observations, which are later used to classify thermalization in quantum systems, are also developed. In chapter 3 the closed quantum system which is analyzed in this thesis, namely the anisotropic Heisenberg ladder, and its Hamiltonian and key observables are introduced. Furthermore, numerical methods such as the Runge-Kutta and Chebyshev expansion, which are used to solve the Schroedinger equation for this system, are introduced and discussed in terms of efficiency, errors and initial states. Chapter 4 presents the results of solving the Schroedinger

equation for the anisotropic Heisenberg ladder and their comparison to the expectations for thermodynamic behavior. Also the eigenstate thermalization hypothesis is checked for this quantum system and the novel method for this which does not rely on exact diagonalization but rather on pure typical quantum states is introduced. In chapter 5 the consistent history formalism is discussed as a possible interpretation of quantum mechanics which can assign probabilities to a sequence of projective measurement outcomes on a closed quantum system. On a rather simple example quantum system it is checked whether Markovian dynamics can be achieved on the level of single measurements using the consistent history formalism.

During my time at the university Osnabrueck I also worked on the topic of transport in disordered quantum systems. Because this is only a small part of my work and loosely connected to the topic of equilibration, the discussion of transport phenomena in random quantum systems is omitted here. It can be found in [28] (see also the list of my publications in Appendix B).

2. Concepts of Equilibration and Unique Equilibration

In this chapter the fundamental concepts regarding equilibration and unique equilibration will be discussed. First of all these terms will be defined by means of a phenomenologically derived system of axioms, which will be later applied to a quantum system. Then concepts and mechanisms of equilibration and unique equilibration for quantum systems, which are already present in the literature, will be presented. These include the "eigenstate thermalization hypothesis", adding extra terms to the Schroedinger equation and a discussion of open quantum systems.

2.1. Axiomatic description of equilibration dynamics

From a phenomenological viewpoint unique equilibration can be defined by considering a scenario which is archetypal for non-equilibrium thermodynamics: Imagine two macroscopic bodies which are coupled to one another but are isolated from the environment. They are prepared at time $t = 0$ in a way that a coarse, macroscopic observable like the temperature difference (or particle number difference, pressure difference and so on) between the two bodies (which will be called x from now on) is non-zero. With this gedankenexperiment based on the every day experience of thermodynamics the key aspects of unique equilibration can be determined. The dynamic of the above mentioned observable x in such a system has a unique, attractive fixed points and is autonomous and Markovian, too. This means that the dynamics of x are free of memory effects, independent of its initial value at time $t = 0$ and are not effected by any other variables.

Thus it can be described by a first-order differential equation of the form

$$\dot{x} = -R(x)x \tag{2.1}$$

If we, for example, choose that the two bodies are a hot and a cold cup of coffee with x being the temperature difference then (2.1) is Newton's law of cooling.

With this in mind the difference between unique equilibration and equilibration can be described quite easily: While "unique equilibration" means that for all initial values of x the same long-term value is reached by Markovian dynamics, "equilibration" is a much weaker condition: For a system to equilibrate not all dynamics starting from different initial values have reach the same long-term value nor need equilibration dynamics to be Markovian and free of memory effects.

Since x is in some sense a statistical variable (its a coarse observable averaged over microscopic dynamic of a large number of microscopic constituents of the two bodies) its variance can be defined as $\sigma^2 = \langle x^2 \rangle - \langle x \rangle^2$. If we would prepare a large number of this experiments in the same initial state regarding x and compare their dynamics no differences would be measurable. Thus σ^2 is small compared to the overall scale of the expectation values of x in the macroscopic limit.

Let us now assume that x has a discrete spectrum of possible values (or a continuous which is then coarse grained). Because of the statistical nature of x and its Markovian dynamics another demand for thermalization dynamics in this sense is that the probability $P_x(t)$ of measuring a certain value of x during its dynamics is described by a (Pauli) master equation

$$\frac{d}{dt}P_x(t) = -\sum_{x'} R_{x,x'}P_{x'}(t) \tag{2.2}$$

where R is matrix with transition probabilities $R_{x,x'}$ from x' to x. Conservation and normalization of probability require the following conditions on R.

$$\sum_{x} R_{x,x'} = 0 \tag{2.3}$$

$$R_{x',x'} = -\sum_{x \neq x'} R_{x,x'} \tag{2.4}$$

Since (2.2) is a valid description of all possible Markovian processes, a criterion for classifying a quantum dynamic as a one with dynamics in accordance with thermody-

namics will be the possibility to find a matrix R so that (2.2) generates a dynamic for $P_x(t)$ which is in accordance with quantum dynamics for $\langle x \rangle$ and σ^2. All in all, the above considerations describe a "recipe" for comparing actual quantum dynamics of an observable which is analogue to the one described in the example above to phenomenological understanding of macroscopic thermodynamic behavior:

- **Unique Equilibration**: Do the dynamics of an observable x feature an unique, attractive fixed point and are they Markovian and free of memory effects (Fig. 2.1 shows an illustration of such behavior)?

- **Autonomy**: In the limit of large system is the variance σ^2 small compared to scale on which the dynamics of x happen?

- **Stochasticity**: Can the dynamics be described by a Pauli master equation (2.2) and what assumptions have to be made about the structure of matrix R?

Note that third criterion "stochasticity" is expected to be true from experience with well understood phenomenons like Brownian motion, but is in this scenario experimentally inaccessible because the autonomy criterion masks all stochastic behavior on a macroscopic scale. Before these hypotheses are tested theories about the mechanisms of equilibration and thermalization of quantum systems already present in the literature will be discussed.

2.2. Equilibration in Quantum Systems

As mentioned above "equilibration" can be defined as the dynamics of a certain observable having an attractive fixed point but this fixed point need not be unique. Furthermore, nothing is said about how this fixed point is reached such that the dynamics need not be Markovian, etc. as is demanded in the above definition for thermalization.

For quantum systems the notion that equilibration exits may seem confusing at first since the time-dependent Schroedinger equation does not feature any fixed point at all. While this is true, it is possible to find equilibrating systems by imposing a condition on the Hamiltonian $\hat{H}$, which has been shown in [29, 13, 30].

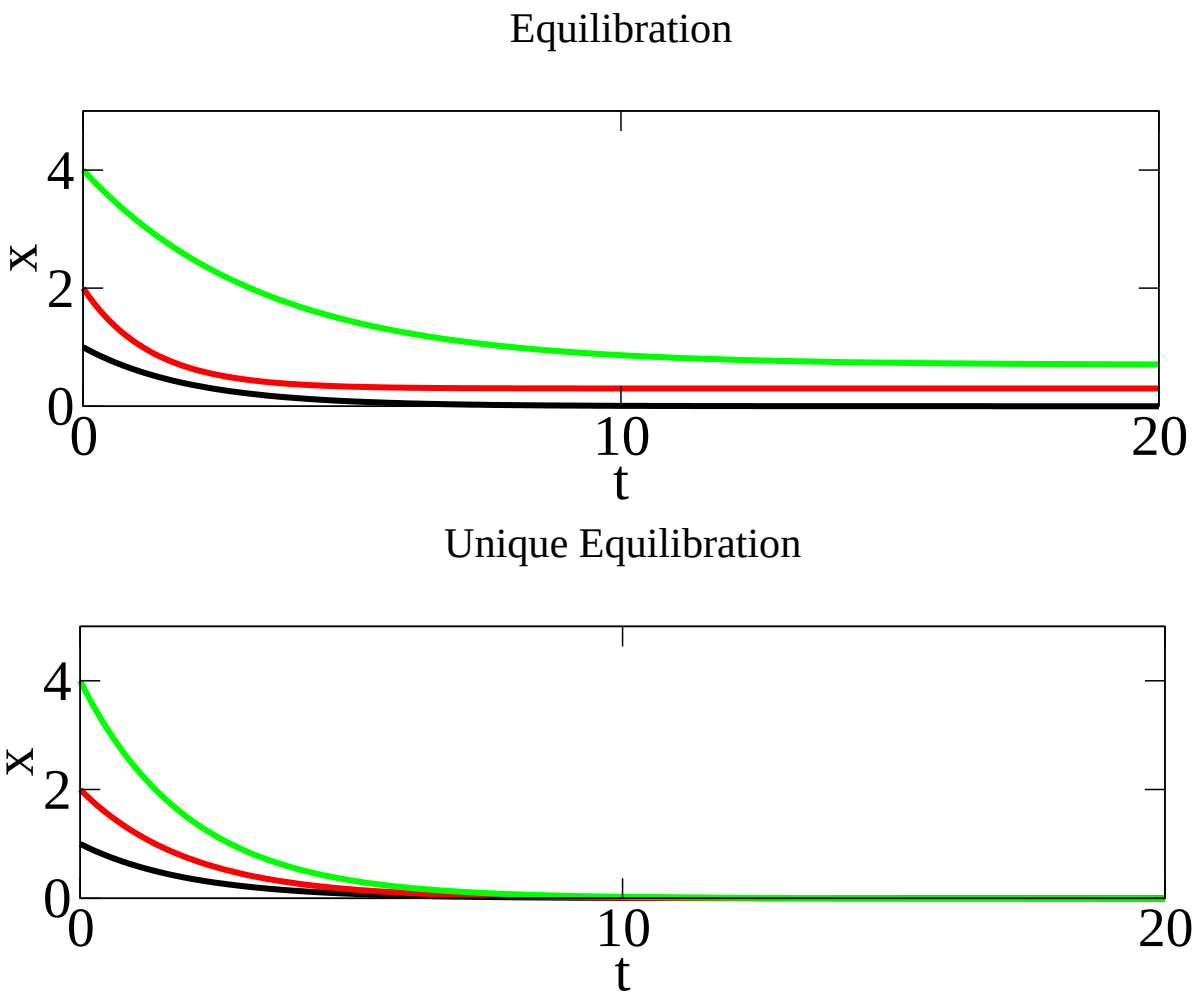

Figure 2.1.: A sketch illustrating the difference between equilibration and unique equilibration. While the system with unique equilibration features an unique, attractive fixed point, so that all dynamics relax towards the same equilibrium value regardless of initial state with the same relaxation constant, this is not the case for system which just equilibrates.

The only assumption about the Hamiltonian needed is that it has non-degenerate energy gaps, which means, given energy eigenvalues E_k, E_l, E_m, E_n of the Hamiltonian, the following expression is true

$$E_k - E_l = E_m - E_n \Rightarrow (E_k = E_l \text{ and } E_m = E_n) \text{ or } (E_k = E_m \text{ and } E_l = E_n) \tag{2.5}$$

Equation (2.5) means that choosing two pairs of eigenvalues with four different indices they cannot have the same energy distance from one another, thus eliminating ,for example, the harmonic oscillator from quantum systems able to show equilibration. Note that systems with degenerate eigenvalues (which arise from symmetry for example) are still viable for fulfilling (2.5). However, this condition means that given a Hamiltonian $\hat{H}$ and two arbitrary decompositions of this system $\hat{H}_A, \hat{H}_B$ the Hamiltonian cannot be of the form $\hat{H} = \hat{H}_A \otimes I_B + I_A \otimes \hat{H}_B$ with I the identity. Thus, any possible decompositions of the Hamiltonian are coupled or all subsystems interact with each other if you will.

With the assumption (2.5) fulfilled for a given Hamiltonian $\hat{H}$, the time average of a quantum observable $\hat{x}$ in a state $|\psi\rangle$ $\overline{x} = \langle\psi(t)|\hat{x}|\psi(t)\rangle_t$ can be computed. Let $E_i\rangle$ denote an eigenstate of the Hamiltonian then the time evolution of $|\psi\rangle$

$$|\psi(t)\rangle = \sum_n c_n e^{-iE_n t/\hbar}|E_n\rangle \tag{2.6}$$

with $c_n = \langle\psi(0)|E_n\rangle$ the weight of $|\psi\rangle$ in the eigenbasis of the Hamiltonian. Then

$$\begin{aligned}
\overline{x} &= \langle\psi(t)|\hat{x}|\psi(t)\rangle_t && (2.7)\\
&= \langle\sum_{n,m} c_m^* c_n e^{i(E_m - E_n)t/\hbar}\langle E_m|\hat{x}|E_n\rangle\rangle_t && (2.8)\\
&= \sum_{n,m} c_m^* c_n \langle e^{i(E_m - E_n)t/\hbar}\rangle_t \langle E_m|\hat{x}|E_n\rangle && (2.9)\\
&= \sum_n |c_n|^2 \langle E_n|\hat{x}|E_n\rangle && (2.10)
\end{aligned}$$

Thus, the “equilibrium value“ of $\hat{x}$ is determined only by the diagonal elements of $\hat{x}$ in the energy eigenbasis of the Hamiltonian and the weight of the initial state in the energy eigenbasis. In [29], there is an estimation of the deviation of the actual expectation value of the observable $\hat{x}$ from the expectation value of $\hat{x}$ with the time averaged equilibrium quantum state. This is essentially a variance of the equilibrium expectation value or a measure of the ”noisiness“ of the quantum dynamics. Let $|\xi\rangle = \langle\psi(t)\rangle_t$ denote the time

averaged (or equilibrium) state then its deviation is

$$\sigma^2_{x,\mathrm{av}} = \langle |\langle\psi(t)|\hat{x}|\psi(t)\rangle - \langle\xi|\hat{x}|\xi\rangle|^2\rangle_t \leq \frac{(\Delta\hat{x})^2}{4d_{\mathrm{eff}}} \leq \frac{||\hat{x}||}{d_{\mathrm{eff}}} \tag{2.11}$$

with $||\cdot||$ the standard operator norm, $(\Delta\hat{x})$ the range of eigenvalues of $\hat{x}$ and

$$d_{\mathrm{eff}} = \frac{1}{\sum\limits_n |\langle\psi(0)|E_n\rangle|^4} \tag{2.12}$$

the "effective dimension" or the dimension of the supporting energy subspace which can range from $1 \leq d_{\mathrm{eff}} \leq \dim\hat{H}$. It equals one if $|\psi(0)\rangle$ is an energy eigenstate of the Hamiltonian and it equals the dimension of the Hamiltonian if the initial state occupies every energy eigenstate of $\hat{H}$ with equal probability. Thus, (2.11) is a strict mathematical formulation of a very intuitive physical concept: The more the initial state is "smeared" in the energy domain, the less noisy the quantum dynamic will be and thus, the actual dynamic will stay very close to the equilibrium value in the long time limit.

In [29, 13] it is argued that for macroscopic systems the dimension of the Hilbert space will be of the order $10^{10^{23}}$ and that a realistic measurement would have much less possible outcomes leading to the impossibility to differentiate the actual quantum dynamic from the time averaged one (respective to a trace distance regarding a measurement) because the distinguishability has the quotient of possible measurement outcomes and and the square root of the effective dimension as an upper bound. Note that in such a scenario that even if the energy of the system is constrained to an interval with width $10^{-10^{22}}$ J the effective dimension will still be of the order of $10^{0.9\cdot 10^{23}}$. Furthermore, a statement regarding the "universality" of the equilibrium state is made in [29]: If a subspace of the Hilbert space with a large effective dimension is chosen and all eigenstates of the Hamiltonian lying in this subspace cannot be distinguished regarding the realistic measurement, then all states within this subspace will equilibrate towards the same equilibrium state.

While the importance of the non-degeneracy condition (2.5) brings deeper understanding to equilibration processes in quantum mechanics with mathematical rigidity and the "universality of equilibration" seems to be a precursor to unique equilibration, this theory has some shortcomings: Nothing is said about the dynamics towards the equilibrium state (of which several may exist) which shape plays an important role to make the

connection from quantum mechanics to non-equilibrium thermodynamics. Furthermore, all conditions and estimations remain on a very abstract layer of quantum mechanics making it impossible to assess if usual Hamiltonians considered in quantum mechanics with number of degrees of freedom much small than 10^{23} (for example electronic or spin systems) fit these categories. Another shortcoming of this theory is that it makes no assumptions about the time scales of the equilibration process: A hot cup of coffee in a cold room which equilibrates on time scales of minutes our hours is not discriminated from the Kepler problem of the earth moving around the sun which equilibrates only on time scales of the heat death of the universe. But the latter would be constituted a non-equilibrating system because of its quasi infinite time scale of equilibration.

2.3. Eigenstate Thermalization Hypothesis

In the previous section the non-degeneracy condition (2.5) was introduced and it was shown that quantum dynamics in form of $\langle \hat{x}(t) \rangle$ equilibrate towards the linear combination of the diagonal elements of $\hat{x}$ in the energy eigenbasis if the energy support of the initial state is large enough. If this process is not merely an equilibration process but unique equilibration is taking place, then all possible initial states from an narrow energy window should relax towards the same equilibrium value of $\langle \hat{x}(t) \rangle$. A theory proposing a mechanism for this feature is the eigenstate thermalization hypothesis (ETH): It states that the microcanonical ensemble in the same energy window as the initial state and the superposition of the diagonal elements of $\hat{x}$ give rise to the same prediction of the equilibrium value of $\langle \hat{x} \rangle$.

$$\sum_n |c_n|^2 \langle E_n|\hat{x}|E_n\rangle = \langle \hat{x} \rangle_{\text{microcan}}(E_0) = \frac{1}{Z} \sum_{n \text{with} |E_0 - E_N| \leq \Delta E} \langle E_n|\hat{x}|E_n\rangle \tag{2.13}$$

with the left hand side the equilibrium value according to the non-degeneracy condition and the right hand side the equilibrium prediction of the microcanonical ensemble where Z is a normalization constant (the number of energy eigenstates in the energy window), E_0 the center of the energy window and ΔE its width. While the right hand side of (2.13) is thermodynamically universal since it only depends on the center and width of the chosen energy window or "temperature" of the quantum system, the left hand side may strongly depend on detailed features of the initial state in form of the c_n. Therefore,

the question how this equality is achieved is very interesting. The assumption the ETH is the following: It is assumed that for states very close in terms of the energy distance the $\langle E_n|\hat{x}|E_n\rangle$ do not or only very little vary giving rise to same equilibrium value regardless of the distribution of the c_n in this energy window [1]. This scenario was proposed in [16] and [17] and has since then been tested on a variety of different quantum systems [16, 18, 31, 32] (including random Hamiltonians, hard-core bosons, quantum billiards). Note that the ETH is merely a hypothesis and there are up to present day only numerical tests (using exact diagonalization) whether a concrete Hamiltonian fulfills the ETH and no abstract proofs.

Assuming the ETH is fulfilled for a certain quantum system and observable the mechanism of unique equilibration can be understood quite easily: The system will thermalize if the chosen energy window of the initial states considered is small enough so that the diagonal elements of the observable in the energy eigenbasis do not vary too much (Note that arbitrary large deviations are allowed on scales of the whole energy spectrum), but the effective dimension (2.12) is large enough so that the dynamics of the observable stays close to its long-time average. As in the equilibration theory of Reimann et al. time plays an ancillary role as the destroyer of coherence between the eigenstates encoded in the initial states. Therefore the ETH lacks any assumptions about the way into equilibrium for which the off-diagonal elements of $\hat{x}$ in the energy eigenbasis are responsible.

2.4. Non-Linear von Neumann Equation

While the last two sections focused on the discussion of conditions imposed onto Hamiltonians such that equilibration and thermalization in terms of the ETH can be achieved, there is also the idea that the standard equations of motion of quantum mechanics have to be modified by adding a non-linear, "dissipative" term which ensures thermalization [33, 3]. The suggested form of the modified von-Neumann equation is

$$\frac{d\rho}{dt} = -\frac{i}{\hbar}[\hat{H}, \rho] + \frac{1}{2k_B\tau(\rho, t)}\{\Delta M(\rho, t), \rho\} \tag{2.14}$$

[1] Note that the opposite scenario would also fulfill (2.13): If the diagonal elements would vary strongly in the energy window but the c_n would not for all initial states in this energy window the same result is achieved. But this seems unlikely

where ρ denotes the standard density operator, $[\cdot,\cdot]$ and $\{\cdot,\cdot\}$ are the standard commutator and anti-commutator, k_B is the Boltzmann constant, $\Delta M(\rho,t)$ is a hermitian operator-valued function of ρ (with $\mathrm{Tr}(\Delta M\rho)=0$ to preserve normalization) and time and $\tau(\rho,t)$ is a positive definite functional of the density operator and time. The function ΔM depends on ρ through the so-called "entropy operator" whose expectation value is the von-Neumann-entropy and on the Hamiltonian itself ensuring a positive rate of entropy generation and relaxation towards an equilibrium density matrix which resembles the density matrix of the grand canonical ensemble (see [33] for details).

While this approach yields a possible mechanism of emergence of thermal states, it will not be considered any further during this thesis since it seems evident from experimental knowledge that the standard equations of quantum mechanics hold. Furthermore, the addition to the standard von-Neumann equation in (2.14) is rather ad hoc and only based on the idea that during thermalization the entropy should increase with time and is not based on a strict mechanical picture.

2.5. Open quantum systems

Another approach to thermalization in quantum systems is to consider a quantum system which consists of two parts: A so-called "bath" or "reservoir" which is assumed to be of infinite size or very large compared to the second part which is most often called the "system". The dynamics of the system alone are then analyzed while tracing out the degrees of freedom of the bath.

A famous example for this is the Caldeira-Legett model [21]. The goal of this paper is to construct a "system + bath" quantum system in which the dynamics of the system follow a Langevin equation

$$m\ddot{x}+\nu\dot{x}+\frac{dV}{dx}=F(t) \tag{2.15}$$

for the position x in the classical limit with the random force $F(t)$ $\langle F(t)\rangle=0$, $\langle F(t)F(t')\rangle = 2\nu k_BT\delta(t-t')$, ν the friction coefficient/relaxation constant and $V(x)$ and external potential acting upon the system part which consists of a single particle. Equation (2.15) is well-known for the description of the Brownian motion of a single particle in a liquid for which the authors are trying to find a quantum analogon in the classical limit.

In [21] a Hamiltonian consisting of a single particle acted upon an external potential $V(x)$ which is coupled to an infinite number of harmonic oscillators is considered:

$$\hat{H} = \frac{\hat{p}^2}{2M} + V(\hat{x}) + \hat{x}\sum_k C_k \hat{R}_k + \sum_k \frac{\hat{p}_k^2}{2m} + \sum_k \frac{1}{2} m\omega_k^2 \hat{R}_k^2 \tag{2.16}$$

with M the mass of the Brownian particle, m the mass of the harmonic oscillators and C_k the coupling constants of the harmonic oscillators to the single particle.

Given this Hamiltonian and the assumptions that the bath of harmonic oscillators is at thermal equilibrium at time $t = 0$ with temperature T, $k_B T >> \hbar\omega_k$ and assuming that the density of harmonic oscillators as a function of the frequency is

$$\rho(\omega) = \frac{2m\nu\omega^2}{\pi C^2(\omega)} \tag{2.17}$$

if $\omega < \Omega$ and zero otherwise (Ω is a cut-off frequency) with $C(\omega)$ the coupling constant between system and bath as a function of the frequency the Langevin equation can be reproduced in the classical limit.

While this theory addresses the dynamics into equilibrium and reproduces the Langevin equation in the classical limit, only open quantum systems are addressed, but ultimately most real world systems are considered to be closed quantum systems which are not coupled to an infinite bath. Furthermore, the question how the bath reached a thermal state is also not addressed and the relaxation constant ν is inducted in this theory by (2.17) as a free parameter rather than being an internal property of a (closed) quantum system.

3. Hamiltonian of the anisotropic Heisenberg ladder and numerical methods

In the previous chapter an axiomatic description of unique equilibration in the macroscopic (as it is observed in the real world) sense is given and existing theories of equilibration and thermalization are discussed. As an introductory example a system consisting of parts sharing a spatial inhomogeneity concerning a certain observable was discussed. Both parts of the system interact with each other, but are isolated from the environment. In this chapter a closed quantum system resembling this gedankenexperiment is given and analyzed in form of an anisotropic Heisenberg spin ladder with the difference of magnetization between the two sides of the ladder as the observable of interest. At first the properties of this system are discussed and the methods of solving the Schroedinger equation in terms of exact diagonalization, Runge-Kutta-scheme and Chebyshev expansion are presented. The dynamics of this setup are then compared to the axiomatic description of unique equilibration in sec. 2.1 and it is tested whether this system fulfills the eigenstate thermalization hypothesis for magnetization difference in the analyzed parameter space.

3.1. Anisotropic Heisenberg Ladder

Our system of choice consists of two anisotropic Heisenberg chains which are coupled to each other. The anisotropic Heisenberg model (sometimes also called “XXZ model”) is a generalization of the Heisenberg model which was invented in the 1920s by Werner

Heisenberg to explain ferromagnetism. Its Hamiltonian reads

$$\hat{h} = J \sum_i \hat{S}_x^i \hat{S}_x^{i+1} + \hat{S}_y^i \hat{S}_y^{i+1} + \Delta \hat{S}_z^i \hat{S}_z^{i+1} \tag{3.1}$$

with $\hat{S}_{x,y,z}^i$ the respective component of the i-th spin operator fulfilling $[\hat{S}_x^i, \hat{S}_y^j] = i\hat{S}_z^i \delta_{ij}$ with eigenvalues $\pm 1/2$ considering spin-1/2 particles. The anisotropy parameter Δ controls how much stronger the z-z-coupling is compared to the other couplings. For $\Delta = 1$ (3.1) becomes the standard Heisenberg model while for $\Delta \to \infty$ it becomes the Ising model and in the limit $\Delta = 0$ it becomes the XY model.

Our system of choice consists of two such Heisenberg chains (3.1) which are coupled in the same manner as in (3.1) but multiplied with a factor κ.

$$\hat{H} = \hat{h}_{\text{left}} + \hat{h}_{\text{right}} + \kappa \hat{V} \tag{3.2}$$

where $\hat{h}_{\text{left}}$ and $\hat{h}_{\text{right}}$ denote the left/right anisotropic Heisenberg chain and $\hat{V}$ represents the coupling between the two parts of the ladder which is

$$\hat{V} = \sum_i \hat{S}_x^{L,i} \hat{S}_x^{R,i} + \hat{S}_y^{L,i} \hat{S}_y^{R,i} + \Delta \hat{S}_z^{L,i} \hat{S}_z^{R,i} \tag{3.3}$$

with L, R denoting that the spin is from the left/right part of the ladder. A coupling $\kappa << 1$ represents the situation where the dynamics within the individual chains are much faster than the dynamics between the chains, which was addressed in the introductory example.

A suitable choice for a basis is the tensor product of the eigenstates of the individual $\hat{S}_z^i$ operators

$$|\mathbf{m}\rangle = |m_1^L m_2^L \dots m_{N/2}^L m_1^R \dots m_{N/2}^R\rangle \tag{3.4}$$

with L, R denoting the left/right part of ladder, N the number of spins in the whole ladder and $m_i^\alpha = \pm 1/2$ denoting the eigenstates of an individual $\hat{S}_z^{\alpha,i}$. Considering this, it is easy to see that the Hilbert space of this problem has the dimension $\dim\mathcal{H} = 2^N$. Therefore, further simplification is needed to make the spin ladder (at least for moderate sized number of spins) feasible for numerical computation. Let $\hat{S}_z^{\text{total}}$ denote the total

magnetization along the z-axis of the system defined as

$$\hat{S}_z^{\text{total}} = \sum_{\alpha=L,R} \sum_i \hat{S}_z^{\alpha,i} \tag{3.5}$$

By means of direct computation it can easily be seen that

$$[\hat{H}, \hat{S}_z^{\text{total}}] = 0 \tag{3.6}$$

which means that the total magnetization along the z-axis is a conserved property in the anisotropic Heisenberg ladder. Thus, the individual subspaces of the Hilbert space with different eigenstates of the total magnetization along the z-axis are independent from one another and we are free to analyze these subspaces individually. Throughout this thesis only the largest of these subspaces with eigenvalue $S_z^{\text{total}} = 0$ is chosen to be the basis, which means that our basis fulfills the constraint

$$\sum_\alpha \sum_i m_i^\alpha = 0 \tag{3.7}$$

With (3.7) the dimension of the $S_z^{\text{total}} = 0$ subspace is found to be

$$\dim \mathcal{H}_{S_z^{\text{total}}=0} = \frac{N!}{\left(\left(\frac{N}{2}\right)!\right)^2} \tag{3.8}$$

which is significantly smaller than 2^N. Furthermore the anisotropic Heisenberg ladder features mirror symmetries which reduces the dimension (3.8) up to a factor 4, but these symmetries are not considered throughout this thesis since they are hard to implement in the existing simulation code and offer only a significant speed up in calculations for small systems using exact diagonalization.

In Table 3.1 the actual size of the $S_z^{\text{total}} = 0$ subspace is listed. From there, it can be seen that sophisticated numerical methods are needed to handle the solution of the Schroedinger equation for larger system sizes. We employ exact diagonalization using the GNU octave library wrapped for C++ up until $N = 16$ for which such a calculation takes about a week on a single core. For intermediate system sizes ($N = 18 \ldots 22$) a Runge-Kutta scheme of fourth order is used with sparse matrices from the Matrix template library (MTL) also on a single core. The largest system sizes ($N = 24 \ldots 32$) are handled by a Chebyshev expansion of the Hamiltonian calculated in parallel on 65536

N	$\dim\mathcal{H}_{S_z^{\text{total}}=0}$
14	3432
16	12870
18	48620
22	705432
26	10400600
32	601080390

Table 3.1.: Dimension of the $S_z^{\text{total}} = 0$ subspace as a function of the number of spins N. Up to 16 spins exact diagonalization is a feasible method for solving the Schroedinger equation. From 18 to 22 spins the Runge-Kutta scheme on a singular core using sparse matrices is employed while from 20 to 32 the parallel Chebyshev expansion is used.

CPUs on IBM BlueGene.Q in Jülich taking about 16 hours of computing time. Details on the inner workings of these algorithms are provided in the next section.

As mentioned in the introduction of this chapter our observable of choice for which unique equilibration will be analyzed is the difference of magnetization between the two parts of the ladder which will be simply called "magnetization difference" from now on. It is defined as the difference of the sum z-component of the spin operator on the left side and the corresponding sum on the right side of the ladder

$$\hat{x} = \sum_i \hat{S}_z^{L,i} - \sum_i \hat{S}_z^{R,i} \tag{3.9}$$

which does not commute with the Hamiltonian (3.2) and which, therefore, is not a conserved quantity in this system. In the basis (3.4) the matrix representation of magnetization difference (3.9) is a diagonal matrix with entries from $-N/2$ to $N/2$ with increment 2. Considering the mirror symmetry of the anisotropic Heisenberg ladder it can easily be seen that for all energy eigenstates of (3.2) $|E_i\rangle$ the expectation value of the magnetization difference is

$$\langle E_i|\hat{x}|E_i\rangle = 0 \tag{3.10}$$

Thus the eigenstate thermalization hypothesis is automatically fulfilled concerning this setup of system and observable and needs no further investigation and only the form of the dynamic of $\langle\hat{x}(t)\rangle$ remains to be investigated.

This particular setup of an anisotropic Heisenberg ladder and magnetization difference as an observable of interest was analyzed in [34] and exponential relaxation for $\langle\hat{x}(t)\rangle$

which was found in the parameter intervals $\kappa \in [0.05; 0.15]$, $\Delta \in [0.5; 0.75]$ by means of exact diagonalization and the time convolution-less super operator projection method for ladders consisting of up to $N = 16$ spins. These findings prompted the idea to further investigate this system for thermalization according to the axiomatic definition in sec. 2.1 and extending the results to larger systems. The results are also published in [27].

3.2. Numerical methods

In this section the numerical methods used for computing the time evolution of the anisotropic Heisenberg ladder, namely exact diagonalization, fourth order Runge-Kutta scheme and the Chebyshev expansion will be discussed. The time-evolved pure state $\psi(t)$ or density operator $\rho(t)$ can be computed from the initial state by

$$\psi(t) = \hat{U}(t)\psi(0) \tag{3.11}$$

$$\rho(t) = \hat{U}(t)\rho(0)\hat{U}^{\dagger}(t) \tag{3.12}$$

with the time-evolution operator

$$\hat{U}(t) = e^{-i/\hbar \hat{H} t} \tag{3.13}$$

which will be exactly determined by exact diagonalization or approximated with the two other numerical schemes. For a detailed review on how to approximate the exponential of a matrix see [35].

3.2.1. Exact diagonalization

To compute (3.13) exactly all eigenstates and corresponding energy eigenvalues of (3.2) must be determined. This is done by diagonalizing the matrix representation of (3.2) in the basis (3.4) using the GNU octave numerical library for C++ which provides a wrapper for linear algebra functions of GNU octave for C++.

Knowing all eigenstates and corresponding eigenvalues of the Hamiltonian expression

the expectation value of an arbitrary operator $\hat{A}$ becomes

$$\langle \hat{A}(t) \rangle = \mathrm{Tr}\left(\hat{A}\rho(t)\right) = \sum_{m,n} e^{i/\hbar(E_m - E_n)} \langle E_m|\hat{A}|E_n\rangle\langle E_n|\rho(0)|E_m\rangle \tag{3.14}$$

with $|E_N\rangle$ the eigenstates of the Hamiltonian and E_n the corresponding energy eigenvalue. The accuracy of this method is only dependent of the accuracy of the method used by the numerical library to determine the eigenstates and eigenvalues which can be assumed to be of the order of magnitude of machine precision. The main disadvantage of exact diagonalization is that it takes a long time to compute all eigenstates and eigenvalues and the corresponding basis transformation of $\hat{A}$ and ρ and the eigenstates have to be stored as dense vectors. A typical calculation for the $N = 16$ anisotropic Heisenberg ladder takes about a week of computing time on a single processor. Since this method's computing costs scale with the third power of the dimension of the Hilbert space it is not feasible for larger systems and approximative methods will be used.

3.2.2. Fourth order Runge-Kutta scheme

The fourth order Runge-Kutta scheme expands the time evolution operator (3.13) into a Taylor series of order 4 and using an iterative calculation of the time evolution which can be written as

$$|\psi(t + \Delta t)\rangle = e^{-i/\hbar \hat{H} \Delta t}|\psi(t)\rangle \tag{3.15}$$

with Δt the time step. Thus, the time evolution from $t = 0$ to $t = t_{\max}$ can be broken down into $t_{\max}/\Delta t$ applications of (3.15). Setting $\hbar = 1$ from now on and expanding the time evolution operator into a Taylor series yields

$$\psi(t + \Delta t) = \left(I - i\Delta t\hat{H} - \frac{\hat{H}^2\Delta t^2}{2} + \frac{1}{6}i\hat{H}^3\Delta t^3 + \frac{1}{24}\hat{H}^4\Delta t^4\right)\psi(t) + O(t^5) \tag{3.16}$$

with I the identity matrix. Equation (3.16) can be brought into a form, which is more efficient for numerical calculation, by splitting up the powers of the Hamiltonian

$$|\psi(t+\Delta t)\rangle = |\psi(t)\rangle + |v_1\rangle + |v_2\rangle + |v_3\rangle + |v_4\rangle \tag{3.17}$$

$$|v_1\rangle = -i\hat{H}\Delta t|\psi(t)\rangle \tag{3.18}$$

$$|v_2\rangle = -1/2i\hat{H}\Delta t|v_1\rangle \tag{3.19}$$

$$|v_3\rangle = -1/3i\hat{H}\Delta t|v_2\rangle \tag{3.20}$$

$$|v_4\rangle = -1/4i\hat{H}\Delta t|v_3\rangle \tag{3.21}$$

Thus, only the vectors $|\psi\rangle$ and $|v_i\rangle$ and the Hamiltonian $\hat{H}$ must be stored during the calculation. Since the Hamiltonian contains a lot of zero entries it is advantageous to save it as a sparse matrix which in this thesis is done by employing the matrix template library (MTL) [36, 37] which provides efficient routines for building and storing sparse matrices and sparse matrix-vector products. This algorithm is usually much faster than exact diagonalization, but has the main disadvantage that due to the Taylor approximation this technique is not exact anymore, but introduces an error due to the cut-off of the Taylor expansion. Furthermore, the time evolution according to (3.17) is not unitary anymore such that the norm of $|\psi(t)\rangle$ is not conserved and will usually decrease with time.

3.2.3. Chebyshev expansion

The second method used in this thesis to compute the time evolution of an Hamiltonian is based on the series expansion of the time evolution operator (3.13) with first-kind Chebyshev polynomials which are defined as

$$T_k(x) = \cos\left(k \arccos\left(x\right)\right) \tag{3.22}$$

with k a natural number. They are orthogonal polynomials on the interval $[-1;1]$. For any $x \in \mathbb{R}$ with $|x| < 1$ it can be shown [38] that

$$e^{-izx} = J_0(z) + 2\sum_{k=1}^{\infty}(-i)^k J_k(z)T_k(x) \tag{3.23}$$

where $J_k(z)$ denotes the Bessel function of the first kind. In order to apply (3.23) to the time evolution operator the eigenvalues of the given Hamiltonian have to be considered: For (3.23) to be applicable all eigenvalues E_i of the Hamiltonian $\hat{H}$ have to lie in the interval $[-1; 1]$ such that that the two-norm of the Hamiltonian fulfills $||\hat{H}||_2 = |\max_i E_i| < 1$. In general this conditions will not be fulfilled by arbitrary Hamiltonians. Therefore a given Hamiltonian has usually to be rescaled in order to apply the Chebyshev expansion. Furthermore, we do not know all eigenvalues of the Hamiltonian and an estimation of the two-norm is needed to be able to rescale the Hamiltonian. An easy estimation of the two-norm is the geometric mean of the one-norm and infinity-norm

$$||\hat{H}||_2 \leq \sqrt{||\hat{H}||_1 \cdot ||\hat{H}||_\infty} \tag{3.24}$$

with

$$||\hat{H}||_1 = \max_j \sum_i |H_{ij}| \tag{3.25}$$

$$||\hat{H}||_\infty = \max_i \sum_j |H_{ij}| \tag{3.26}$$

and H_{ij} the matrix elements of the Hamiltonian given in a certain basis. Other methods of estimating the extreme eigenvalues of the Hamiltonian include iterative eigensolvers like the Arnoldi method which will give a good approximation to the dominant eigenvalue with few iterations.

Having estimated the largest and smallest (by using $-\hat{H}$ in the estimation procedure) eigenvalue of the given Hamiltonian it can be rescaled as

$$\widetilde{H} = \frac{\hat{H} - b}{a} \tag{3.27}$$

with $a = 1/2\,(E_{\max} - E_{\min})$, $b = 1/2\,(E_{\max} + E_{\min})$ and $E_{\max}, E_{\min}$ the estimators of the largest and smallest eigenvalue of $\hat{H}$. With this the time evolution operator can be written in the Chebyshev expansion as

$$\hat{U}(\Delta t) = e^{-i/\hbar \hat{H} \Delta t} \approx e^{-ib\Delta t/\hbar} \left(J_0(a\Delta t/\hbar) + \sum_{k=1}^{M} (-i)^k J_k(a\Delta t/\hbar) T_k(\widetilde{H}) \right) \tag{3.28}$$

with M the maximum order of the Chebyshev expansion and $T_k(\widetilde{H})$ is the matrix-valued Chebyshev polynomial. Thus, to compute $|\psi(t+\Delta t)\rangle = \hat{U}(\Delta t)|\psi(t)\rangle$ M different Cheby-

shev polynomials of the Hamiltonian multiplied by the wave function $|v_k\rangle = T_k(\widetilde{H})|\psi(t)\rangle$ have to be computed and stored. This can be done by employing the recursive definition of the Chebyshev polynomials.

$$|v_{k+1}\rangle = 2\widetilde{H}|v_k\rangle - |v_{k-1}\rangle \tag{3.29}$$

with $|v_1\rangle = \widetilde{H}|v_0\rangle$ and $|v_0\rangle = |\psi(t)\rangle$. Exploiting the fact that the Hamiltonian of the anisotropic Heisenberg ladder contains a large amount of zeros it can be saved in a sparse matrix format for which matrix-vector multiplications like (3.29) are very fast and can be distributed over many different CPUs. The Bessel functions in (3.28) can be computed on time-scales of the order of a fracture of a second and do not contribute significantly to the computing time of this algorithm.

The order of truncation of the series M in (3.28) plays a different role than in the Taylor expansion used for the Runge-Kutta scheme. While the latter the order of magnitude of different terms in the Taylor series can fluctuate strongly leading to the problem of a strong round-off error (it has been argued [35] that the fourth order is the most stable for a Taylor expansion), all terms in the Chebyshev expansion are in the same order of magnitude since all terms in (3.28) have two-norms which are smaller than one. Thus, the accuracy can be improved by increasing M without increasing round-off errors. All calculations using the Chebyshev expansion of the time evolution operator were performed on BlueGene.Q in Jülich. For more details on this algorithm and its applications to other quantum systems see [39, 40, 41, 42, 43, 44, 45].

3.3. Initial states

In the beginning of this chapter the magnetization difference $\hat{x}$ (3.9) was introduced as the observable for which thermodynamic behavior is sought for in the anisotropic Heisenberg ladder. It was further argued that due to symmetry the eigenstate thermalization hypothesis is automatically fulfilled for this observable and that a quantum state with $\langle\hat{x}\rangle = 0$ is in equilibrium regarding the magnetization difference. In order to be able to study possible relaxation towards this equilibrium value the initial state should feature expectation values of the magnetization difference at time $t = 0$ which are different from zero. Furthermore, the energy window of the initial state shall be constrained to a small

portion of the whole energy spectrum. All calculations presented in the following chapter are made for energy intervals centered around $E = 0$ with corresponds to states with infinite temperature.

For calculations using exact diagonalization this can be achieved as follows: Since all eigenvalues and eigenstates are known an energy projector $\hat{P}_{E,\Delta E}$ which projects onto the energy interval $[E - \Delta E; E + \Delta E]$ can easily be constructed in both the "spin-up/spin-down" and the energy eigenbasis. The magnetization difference $\hat{x}$ has eigenvalues ranging from $-N/2$ to $N/2$ with increment two if N is the total number of spins in the ladder. A projector $\hat{P}_x$ onto a certain eigenvalue of the magnetization difference can also be easily constructed in the "spin-up/spin-down" basis. Thus for exact diagonalization initial states

$$\rho = \frac{1}{Z}\hat{P}_{E,\Delta E}\hat{P}_x\hat{P}_{E,\Delta E} \tag{3.30}$$

with Z the normalization which ensures $\mathrm{Tr}\,(\rho) = 1$. At time $t = 0$ these initial states have the expectation values

$$\mathrm{Tr}\,(\rho(0)\hat{x}) \approx x \tag{3.31}$$

$$\sigma^2 = \mathrm{Tr}\left(\rho(0)\hat{x}^2\right) - \mathrm{Tr}\,(\rho(0)\hat{x})^2 \approx 0 \tag{3.32}$$

The approximate signs in (3.31) and (3.32) come from the energy projection which smudges the magnetization difference. Note that initial states (3.30) cannot be constructed for all possible combinations of $E, \Delta E, x$ if (3.31) and (3.32) shall remain valid. If for example $x = N/2$ is chosen, then an energy projection onto the center of the energy spectrum with a small ΔE compared to the overall length of the spectrum leads to a violation of (3.31) and (3.32) and ,thus, an unreasonable initial state.

For calculations using the fourth order Runge-Kutta scheme and the Chebyshev expansion similar but pure initial states shall be used with also feature

$$\langle\psi(0)|\hat{x}|\psi(0)\rangle \approx x \tag{3.33}$$

$$\sigma^2 = \langle\psi(0)|\hat{x}^2|\psi(0)\rangle - \langle\psi(0)|\hat{x}|\psi(0)\rangle^2 \approx 0 \tag{3.34}$$

for x an eigenvalue of the magnetization difference and are constrained to a certain energy window. To construct these initial states the concept of typicality [46, 47] is employed, which can be explained as follows: A set of pure quantum states is given which

share some common feature. If this set of states also gives a narrow distribution of another feature then there is typicality. The shared common feature, for example, could be that the states are drawn at random according to the same distribution and then have a narrow distribution of quantum expectation values for a certain observable. It has been demonstrated [12] that, if pure states are drawn at random from the unitary invariant ensemble (an ensemble of normalized, pure states which are invariant under all unitary transformations in the Hilbert space), typicality can be achieved. From these considerations energy constrained states with a certain expectation value of magnetization difference are constructed by employing

$$|\omega\rangle = \frac{1}{A}\hat{P}_x e^{-\alpha/4\left(\hat{H}-E_f\right)^2}|\psi\rangle \tag{3.35}$$

with $\alpha > 0$ a constant which regulates the width of the energy window of $|\omega\rangle$, A a normalization constant and $\langle\omega|\hat{H}|\omega\rangle = E_f$. The operator $e^{-\alpha/4\left(\hat{H}-E_f\right)^2}$ replaces the energy projector used in constructing the initial states for exact diagonalization since for Runge-Kutta and Chebyshev the eigenvalues and eigenstates of the Hamiltonian are unknown. While the projection operators for energy represent a box filtering of the energy, for Runge-Kutta and Chebyshev a Gaussian filter is applied to the energy. This energy filter is calculated using the same numerical algorithm which is used for the approximation of the time evolution operator, i.e. if the time evolution is calculated by the fourth order Runge-Kutta scheme then the energy filter is also calculated by a fourth order Runge-Kutta scheme (using imaginary time evolution with a Gaussian). This is easily possible since both algorithms rely only on the expansion of an operator into a polynomial series. The state $|\psi\rangle$ is constructed by randomly generating a superposition of all states in the up-down basis with $S_z^{\text{total}} = 0$ and drawing its coefficient's real and imaginary part from a Gaussian random generator. For a detailed discussion on typicality see sec. 4.3 in which typicality and the eigenstate thermalization hypothesis are discussed.

Our analysis of typicality is restricted to the static case so far. This means that we cannot be sure that if two states $|\omega\rangle, |\omega'\rangle$ which are constructed according to (3.35) will feature approximately the same quantum expectation values for the magnetization difference at all times t only because there is typicality at time $t = 0$. This scenario is referred to as "dynamical typicality" and is analyzed in [48] for a set of initial states which are not compatible to the scenario used for the anisotropic Heisenberg ladder. Therefore, this analysis of dynamical typicality also relies on numerical evidence. In Fig.

3.1 the results for $\langle \hat{x}(t) \rangle$ for five different initial states with $\langle \hat{x}(0) \rangle = 2$ for a system comprising $N = 16$ spins with $\Delta = 0.6$ and $\kappa = 0.2$ are depicted. The initial states are constructed according to (3.35) with α chosen such that $\mathrm{Var}\left(\hat{H}\right) = 0.12$. The time-evolution is computed using the Runge-Kutta scheme with a time step $\Delta t = 0.01$. Although the initial states are generated at random according to the unitary invariant

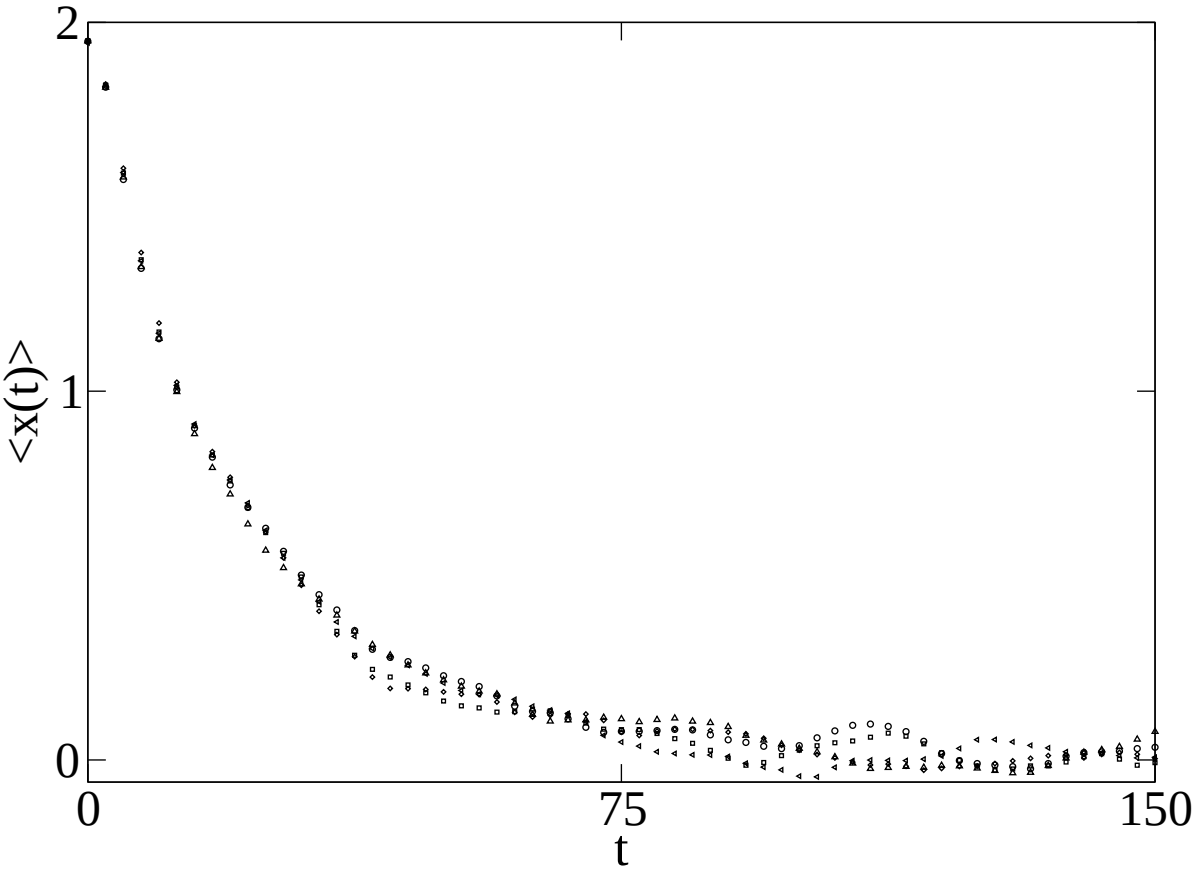

Figure 3.1.: Time evolution of $\langle \hat{x}(t) \rangle$ for five different pure initial states constructed according to (3.35) for a system of $N = 16$ spins with $\Delta = 0.6$, $\kappa = 0.2$ and $\langle \hat{x}(0) \rangle$=2. The time-evolution is computed using the Runge-Kutta scheme with time step $\Delta t = 0.01$. Although these initial states are generated at random with $\mathrm{Var}\left(\hat{H}\right) = 0.12$, the time evolution $\langle \hat{x}(t) \rangle$ is approximately the same for all of them.

ensemble and they differ on the level of individual basis coefficients, the time evolution of the magnetization difference is approximately the same for all five states. Thus, this Hilbert space and the observable magnetization difference show typicality on the static and dynamic level. Therefore, initial states constructed according to (3.35) are used in the analysis of the thermodynamics of the anisotropic Heisenberg ladder.

4. Unique equilibration in the anisotropic Heisenberg ladder

In the previous chapter the Hamiltonian of the anisotropic Heisenberg ladder, the "spin-up/spin-down" basis and its symmetries were discussed. Since the dimension of the Hilbert space of this quantum system scales with the factorial of the number of spins numerical methods of computing the time-evolution which can go beyond exact diagonalization in terms of system sizes were introduced. The initial states used for this numerical methods were also discussed in terms of typicality. This discussion led to the conclusion that although these states are different on the microscopic level (individual basis coefficients), because they are generated at random, they have the expectation value of the magnetization difference as a common macroscopic (in a coarse-grained sense) feature. This corresponds well to the concepts of thermodynamics, in which the macrostate is known but not the microstate. Therefore, these initial states are used in the analysis of the anisotropic Heisenberg ladder. For all numerical analyses in this chapter we choose $\hbar = 1$, $\Delta = 0.6$, $\kappa = 0.2$ and $J = 1$ (the parameter J only sets the energy scale of the system and has no other influence on the dynamics). The parameter α in (3.35) is chosen such that the variance of the energy is $\mathrm{Var}\left(\hat{H}\right) = 0.14$.

As an introductory example of thermodynamic behavior in this quantum system, which will only be analyzed qualitatively, consider the following scenario: For a ladder consisting of $N = 32$ spins two initial states with $\langle \hat{x}(0) \rangle = 8$ and $\langle \hat{x}(0) \rangle = -6$ are chosen which are very far apart from one another in terms of the total range of eigenvalues of magnetization difference. If the system would behave according to standard thermodynamics, both states would reach an equilibrium state. The equilibrium states should be indistinguishable in terms of the macroscopic variable $\hat{x}$. To check the time evolution of such a system is computed with the Chebyshev expansion for the initial states mentioned above and the probability distribution of being in a certain magnetization difference subspace

$P_x(t) = \langle \hat{P}_x \rangle$ is computed. The results of this computation are displayed in Fig. 4.1. There it can easily be seen that although the probability densities are far apart at time

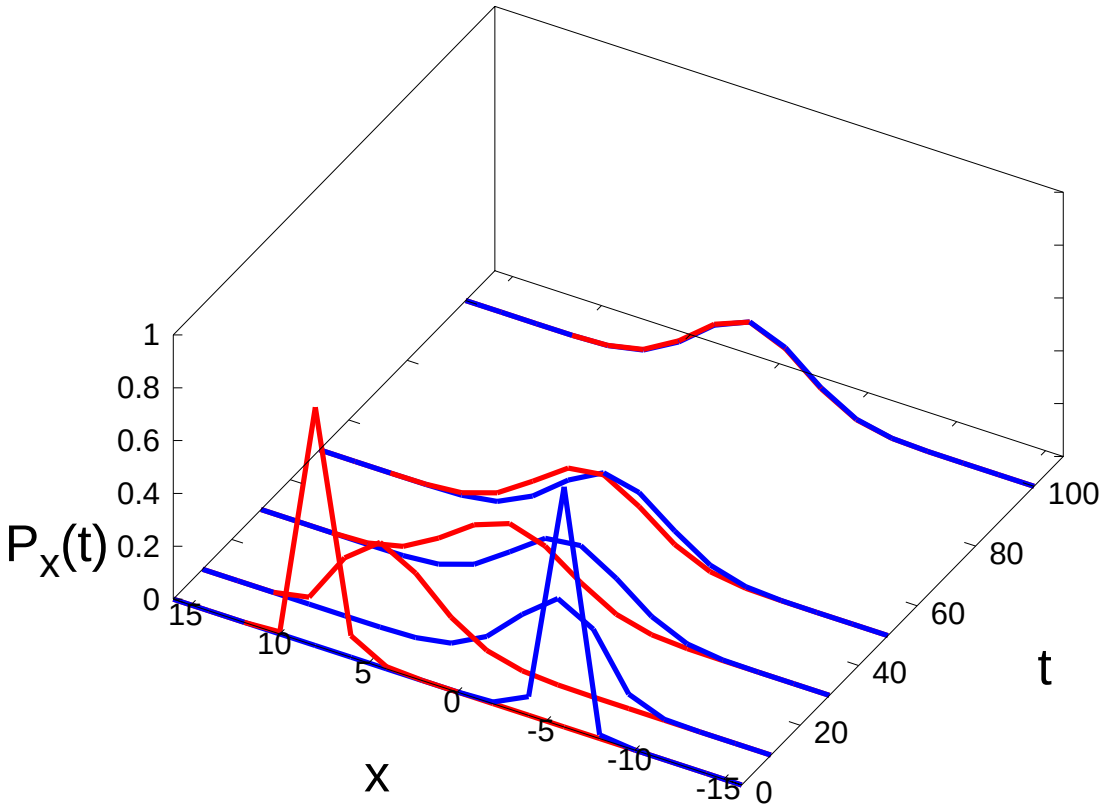

Figure 4.1.: Dynamics of the probability distribution $P_x(t)$ for spin-ladders of size $N = 32$ for two different (partially random) initial states $|\omega\rangle$ with $\langle \hat{x}(0) \rangle = 8$ (red line) and $\langle \hat{x}(0) \rangle = -6$ (blue line). The two probability distributions hardly overlap at $t = 0$ and almost coincide at later times. The time evolution is computed using the Chebyshev expansion.

$t = 0$ they move closer together with time and cannot be discriminated by the naked eye at time $t = 100$. Note that the actual quantum states cannot move closer together in terms of a distance measured by a metric in the Hilbert space because of the unitary dynamic. Furthermore, the distribution is centered at $x = 0$ at this time which is the expected unique equilibrium value.

This analysis shows the possibility of thermodynamic behavior for this quantum system. Therefore, a more quantitative analysis according to the "axioms of thermodynamics" discussed in sec. 2.1 is performed. This means the expectation value of the magnetiza-

tion difference should show Markovian relaxation dynamics while its variance σ^2 should become negligible compared to the overall scale of eigenvalues of the magnetization difference in the limit $N \to \infty$. Furthermore, the dynamics of these two observables should follow a traditional Pauli master equation.

4.1. Dynamics of the mean and variance of the magnetization difference

The first goal is to determine whether the dynamics of the expectation value of the magnetization difference show Markovian and autonomous dynamics. To check this for a given system size N the time evolution $\langle \hat{x}(t) \rangle$ is computed for all different initial magnetization differences $\langle \hat{x}(0) \rangle = 0 \ldots N/2$ (the negative magnetization differences can be ignored due to symmetry). Then the resulting curves are moved on top of each other using a least squares fit: Let us denote two different curves of $\langle \hat{x}(t) \rangle$ with different initial magnetization differences at time $t = 0$ by $y_1(t)$ and $y_2(t)$. Then the expression

$$\sum_i \left(y_1(t_i) - y_2(t_i + h) \right)^2 \tag{4.1}$$

is minimized numerically for the variable h with t_i the discrete time steps generated by the numerical computation of the time evolution. Thus, for every pair of curves a shift parameter h can be computed. For this analysis we start with the highest possible starting magnetization difference and move the smaller ones on top of it. If these dynamics are Markovian, the curves should be indistinguishable from one another after this process. The results of this analysis are depicted in Figs. 4.2 and 4.3. For the setup with $N = 16$ the curves for $\langle \hat{x}(0) \rangle = 2$ and $\langle \hat{x}(0) \rangle = 4$ lie on top of each other very well while the expectation value for $\langle \hat{x}(0) \rangle = 6$ cannot be moved to be in accordance with the other two curves. (higher values of the magnetization difference are omitted here because they have the same problem as $\langle \hat{x}(0) \rangle = 6$ and $\langle \hat{x}(0) \rangle = 0$ is omitted because it has no dynamic at all).

The setup with $N = 32$ is shown for initial magnetization differences up to $\langle \hat{x}(0) \rangle = 12$, which can all be moved on top of each other nicely while higher values of magnetization difference are omitted in this figure since these initial states do not exist in the given

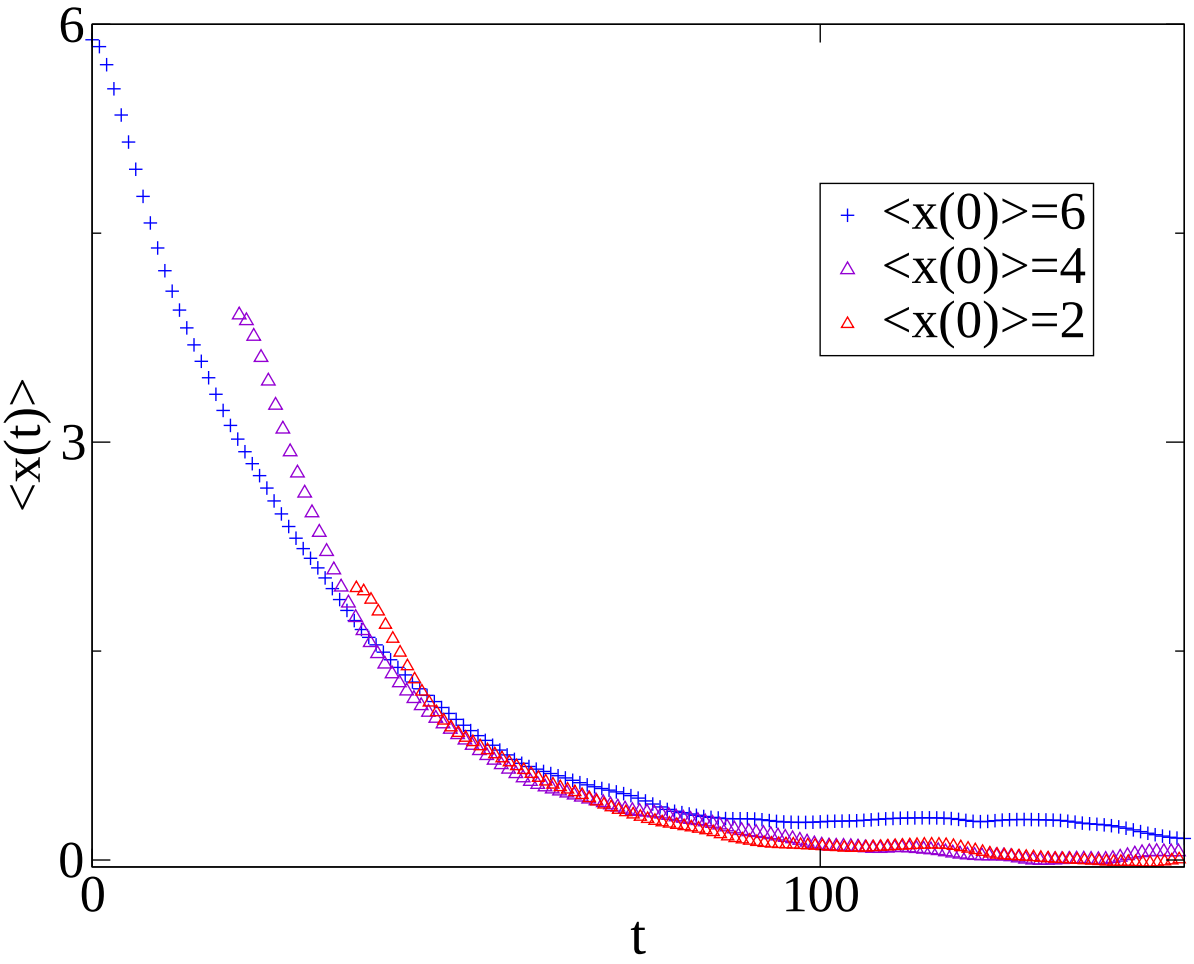

Figure 4.2.: Expectation values $\langle \hat{x}(t) \rangle$ of the magnetization difference for $N = 16$ and three initial states featuring different $\langle \hat{x}(0) \rangle$. Graphs are shifted in time for optimal agreement.

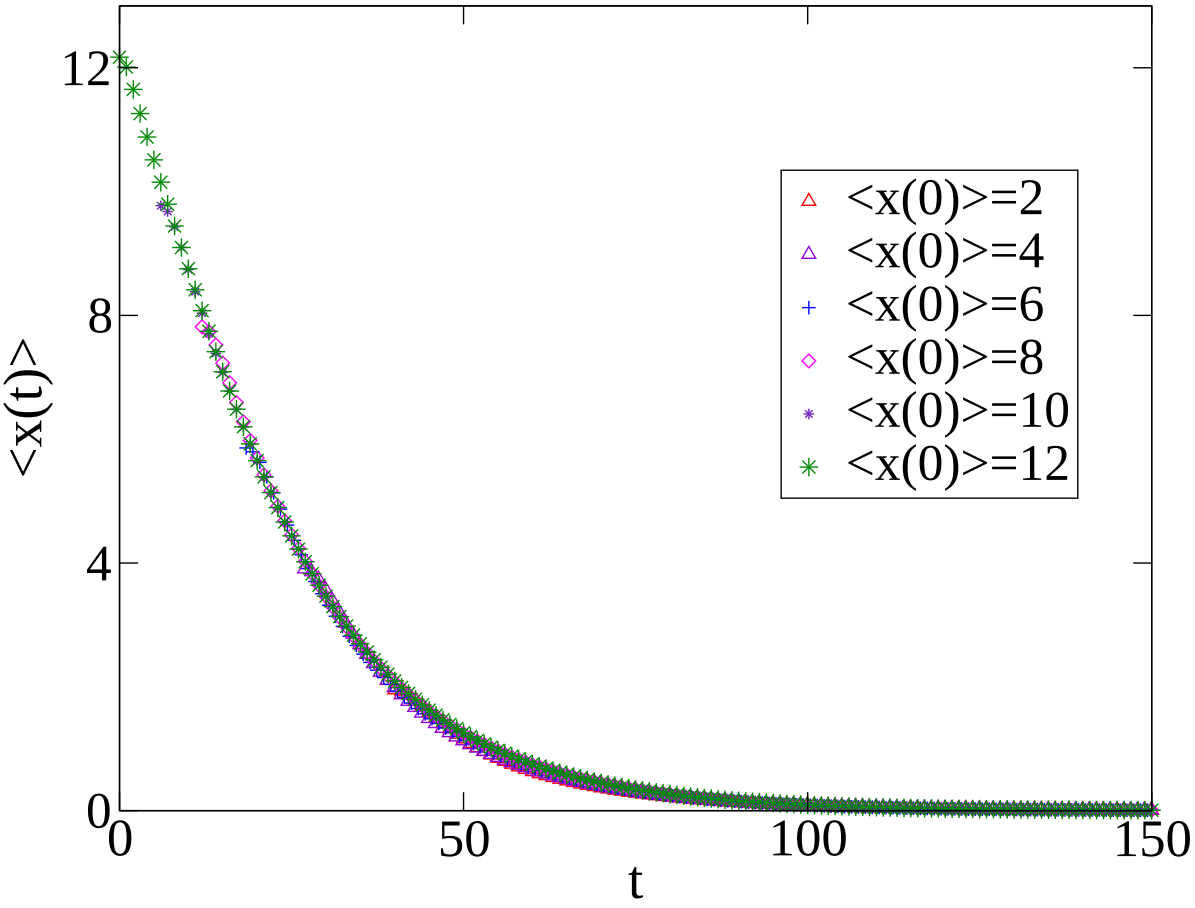

Figure 4.3.: Expectation values $\langle \hat{x}(t) \rangle$ of the magnetization difference for $N = 32$ and four initial states featuring different $\langle \hat{x}(0) \rangle$. Graphs are shifted in time for optimal agreement.

energy shell. In both cases the dynamics of the expectation value of the magnetization difference are Markovian and autonomous for almost all ($N = 16$) or all ($N = 32$) possible initial states in the given energy shell. Therefore, it is a promising task to analyze the dynamics of the variance of the magnetization difference for this system.

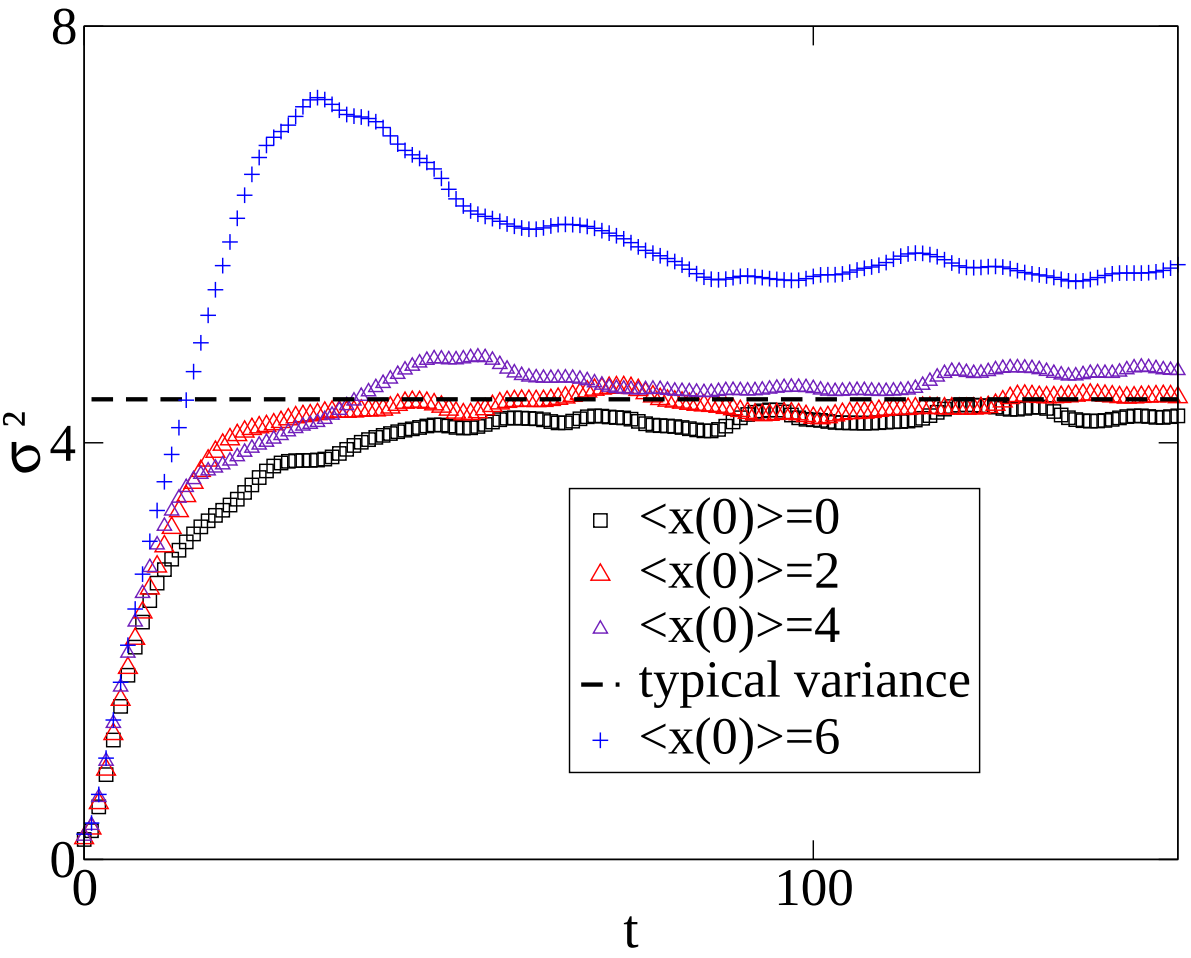

Figure 4.4.: Variances σ^2 of the magnetization difference for $N = 16$ and different initial states regarding the starting value of magnetization difference. The solid line indicates the typical variance.

In Fig. 4.4 and 4.5 the variances of the magnetization difference $\sigma^2 = \langle \hat{x}(t)^2 \rangle - \langle \hat{x}(t) \rangle^2$ are displayed for systems with $N = 16$ and $N = 32$ spins. While the final variances for the system comprising $N = 16$ tend to spread strongly, this effect decreases drastically for a system with $N = 32$ spins for which the final variances lie around the typical variance.

The question why the final values of the variances take on the same value is related to

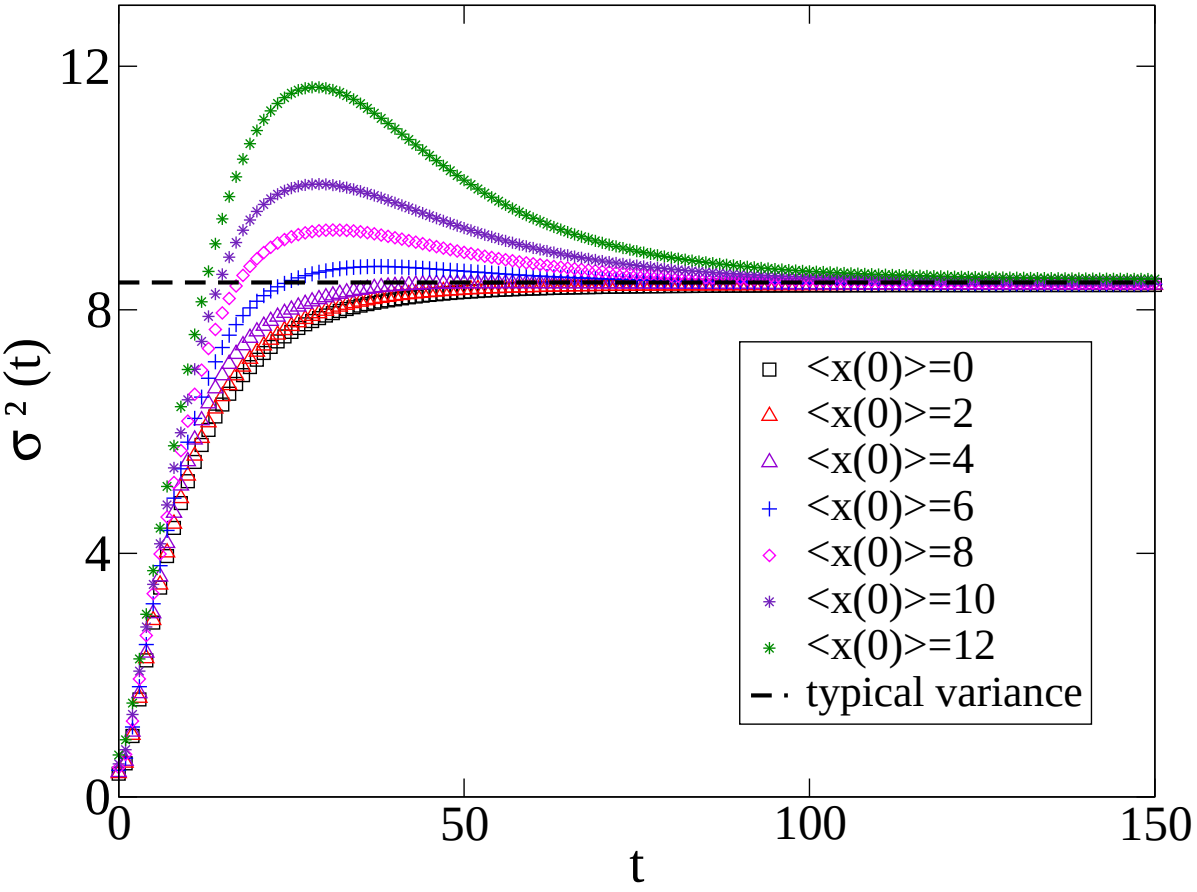

Figure 4.5.: Variances σ^2 of the magnetization difference for $N = 32$ and different initial states regarding the starting value of magnetization difference. The solid line indicates the typical variance.

typicality: The "typical variance" in Fig. 4.4 and 4.5 is the variance of a normalized pure quantum state which is unrestricted with respect to $\langle \hat{x} \rangle$ but energy projected onto the same energy interval used for the states whose time evolution is analyzed:

$$\sigma^2_{\text{typical}} = \langle \varphi | \hat{x}^2 | \varphi \rangle - \langle \varphi | \hat{x} | \varphi \rangle^2 \tag{4.2}$$

$$|\varphi\rangle = \frac{1}{A} e^{-\alpha \left(\hat{H} - E_F\right)^2} |\Psi\rangle \tag{4.3}$$

According to the concept of typicality presented in the previous chapter for systems with small Hilbert space variance in the considered energy shell, there is a huge region in the Hilbert space with states (with respect to the unitary invariant ensemble) featuring a common expectation value for a certain quantum observable while the region with states featuring another expectation value for this observable is tiny. The above coincidence indicates that while all considered initial states start in a very tiny region of Hilbert space formed by "non-typical" states, the states venture out into the extremely large region formed by the typical states, while other initial states (high values of starting magnetization difference for small system sizes) do not.

While the clustering of the final variances around the generic, typical variance which improves with scaling up to system to $N = 32$ spins can be seen as an indicator of thermodynamic behavior, an early maximum of the variance develops which would not be present if $\langle \hat{x} \rangle$ truly behaved like a Brownian particle in a harmonic potential as claimed in [27]. Thus, the dynamics of the variance of the magnetization difference σ^2 is not Markovian and autonomous for the initial states considered here in the sense that the dynamics are independent of the initial value of the magnetization difference. But this was not part of the "thermodynamic axioms". It was rather postulated that the variance should become negligible in the macroscopic limit. Therefore, the scaling of typical variance, final variance and early maximum of the variance with system size have to be analyzed. The results of this analysis are depicted in Fig. 4.6. There the mean of all final variances from initial states is compared to the linear fit of the typical variance. Furthermore, the early maximum is extracted from the largest possible initial state for which it is the largest. It can easily be seen that all these values scale linearly with system size. Thus, the standard deviation of the magnetization difference σ scales like $\sigma \propto \sqrt{N}$, while the range $x_{\max}$ of possible initial states for which the expectation value of the magnetization difference is autonomous and Markovian and the final variance clusters around its typical value scales linearly with system size. Thus, in the macroscopic limit

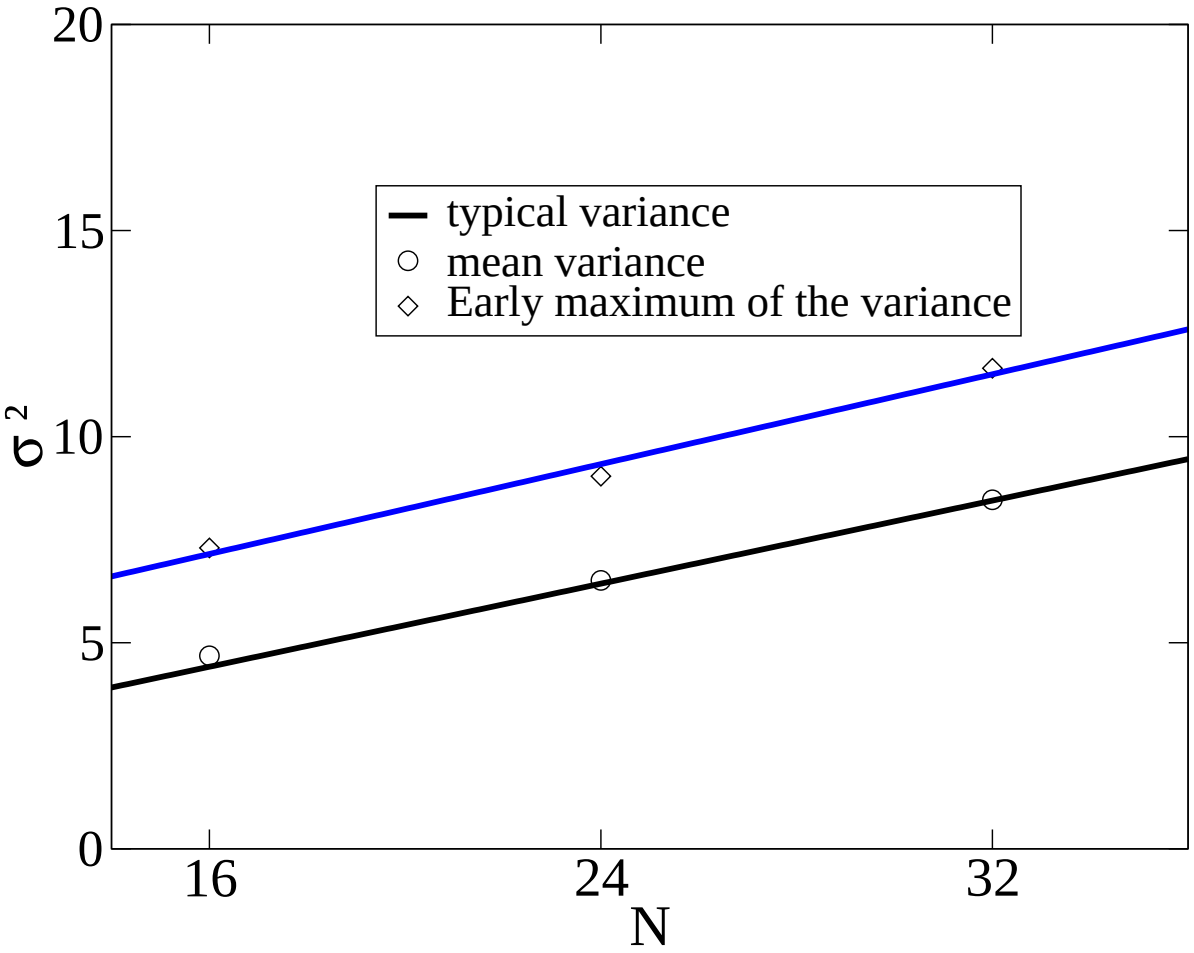

Figure 4.6.: Average of the final variances for different system sizes N sampled from initial states shown in Fig. 4.4 and Fig. 4.5. The early maximum is extracted from the largest existing initial state for the corresponding system size.

$N \to \infty$

$$\frac{\sigma}{x_{\max}} \to 0 \tag{4.4}$$

In other words, the standard deviation becomes negligibly small compared to the possible range of starting magnetization difference values which was one of the "thermodynamic axioms". Thus, for macroscopic systems measurement outcomes for the magnetization difference are quasi deterministic for these initial states.

4.2. Comparison of the dynamics to a Pauli master equation

The last question remaining concerning the validity of calling the anisotropic Heisenberg ladder a thermodynamic system is whether the dynamics of $\langle \hat{x} \rangle$ and σ^2 can be described by a Pauli master equation. This question was first addressed for small systems with up to $N = 16$ spins in [27]. There the quantum dynamics were compared to a Pauli master equation whose rates lead to a Fokker-Planck type behavior meaning exponential relaxation of $\langle \hat{x} \rangle$ and limited exponential growth up to the typical variance for σ^2. While this model gives reasonable agreement with the quantum dynamics for small system sizes and initial states close to equilibrium, it can easily be seen from Figs. 4.7 and 4.8 that such a description cannot remain valid for initial states far-away from equilibrium even for large system sizes because of the developing early maximum of the variance which is not reproduced correctly by this rate equation.

While the above mentioned stochastic model is based on combinatorial considerations regarding the number of up and down spins in both beams of the ladder, now a rather ad-hoc model will be discussed whose rates do not have any physical background but are rather manually chosen to reproduce the quantum dynamics. Therefore, the following setup is considered: The system can only transition from its current magnetization difference subspace in a neighboring one meaning that rates $R_{xy} \neq 0$ only if $x = y \pm 2$. With this the expectation value of magnetization difference $\overline{x}$ (the overline indicates a classical expectation value computed from the probabilities of the individual magnetization difference subspaces generated by the Pauli master equation) can be calculated. If the Pauli master equation is solved and the probabilities of the individual magnetization

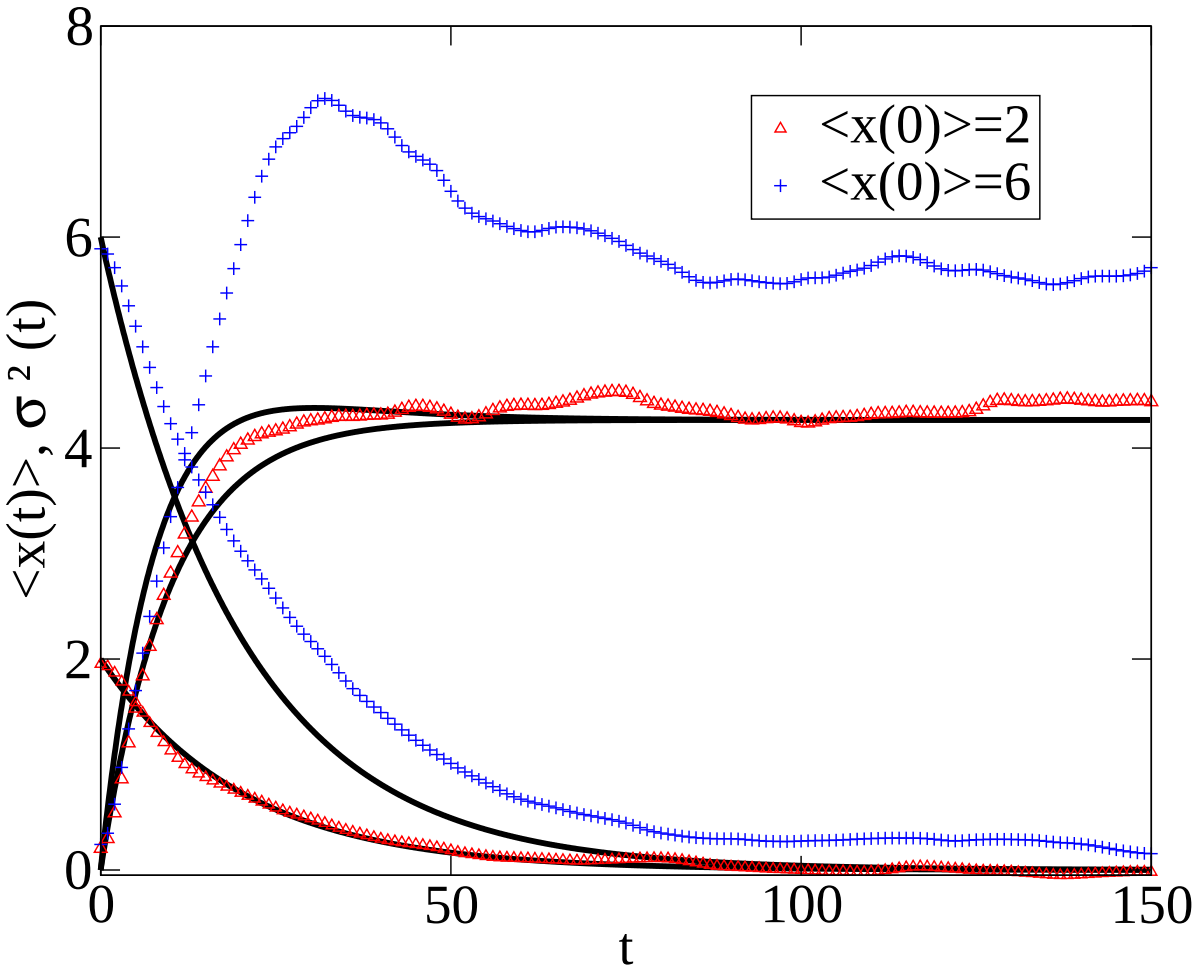

Figure 4.7.: Quantum expectation values $\langle \hat{x}(t) \rangle$ and variances σ^2 of the magnetization difference for $N = 16$ for two states, one starting close to equilibrium $\langle \hat{x}(0) \rangle = 2$ and the other far from equilibrium $\langle \hat{x}(0) \rangle = 6$. Solid lines represent the corresponding data as calculated from the stochastic model suggested in [27]. Close to equilibrium the agreement is good, while more off-equilibrium it is not.

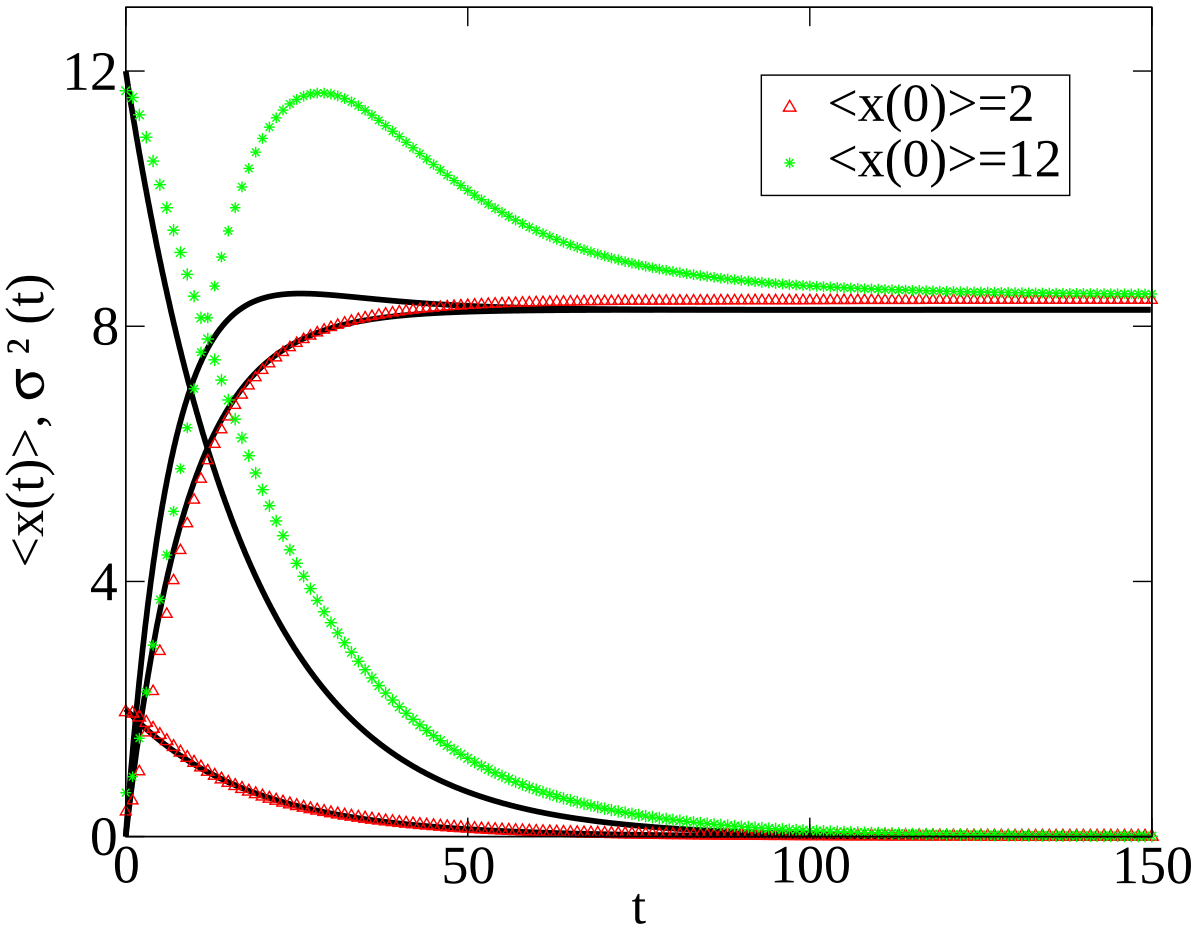

Figure 4.8.: Quantum expectation values $\langle \hat{x}(t) \rangle$ and variances σ^2 of the magnetization difference for $N = 32$ for two states, one starting close to equilibrium $\langle \hat{x}(0) \rangle = 2$ and the other far from equilibrium $\langle \hat{x}(0) \rangle = 12$. Solid lines represent the corresponding data as calculated from the stochastic model suggested in [27]. Close to equilibrium the agreement is good, while more off-equilibrium it is not.

subspaces $P_x(t)$ are known $\overline{x}$ is defined as

$$\overline{x}(t) = \sum_y y P_y(t) \tag{4.5}$$

Since the data from the quantum dynamics suggest that the expectation value of magnetization difference relaxes exponentially $\overline{x}(t)$ shall fulfill

$$\frac{d}{dt}\overline{x}(t) = -G\overline{x}(t) \tag{4.6}$$

with G the relaxation constant which has to be extracted from the quantum data. Plugging the definition of $\overline{x}$ (4.5) into (4.6) yields if the definition of the Pauli master equation is used to eliminate the first temporal derivative of the probabilities

$$\sum_y \left(\sum_x x R_{xy} + Gy \right) P_y = 0 \tag{4.7}$$

This expression can be further simplified and finally yields using the conservation of probability $\sum_x R_{xy} = 0$

$$\sum_x (x - y) R_{xy} = -Gy \tag{4.8}$$

Using the postulated property that only transitions between neighboring magnetization subspaces (which have a distance of two) occur leads to

$$R_{x+2,x} - R_{x-2,x} = -\frac{G}{2}x \tag{4.9}$$

A similar calculation can be performed for the dynamics of the variance σ^2 and relates the sum $R_{x+2,x} + R_{x-2,x}$ to a diffusion coefficient $D(x)$. In case of standard Fokker-Planck dynamics (like a Brownian particle in an harmonic trap) a constant diffusion coefficient wold be chosen, but as it was argued above this is not possible here. Instead, an inverted Lorentzian curve is chosen for the diffusion coefficient without any physical considerations but rather the ad-hoc thought that from looking at Fig. 4.5 the diffusion coefficient should be larger for the outermost magnetization difference subspaces. This leads to the following expression for the rates

$$R_{x+2,x} = 0.5(A + B - B/(1 + (x/C)^2) - Gx) \tag{4.10}$$

$$R_{x-2,x} = 0.5(A + B - B/(1 + (x/C)^2) + Gx) \tag{4.11}$$

where A, B, C, G are parameters which have to be extracted from the quantum dynamics. This is done by using a least squares algorithm which minimizes the deviation of the solution of the Pauli master equation with rates (4.10), (4.11) from the actual quantum dynamics with initial states featuring $|\langle x(0)\rangle| \leq N/4$ (resulting in $A = 0.16$, $B = 0.19$, $C = 2.5$, $G = 0.046$). The results of this process are depicted in Fig. 4.9. The reason-

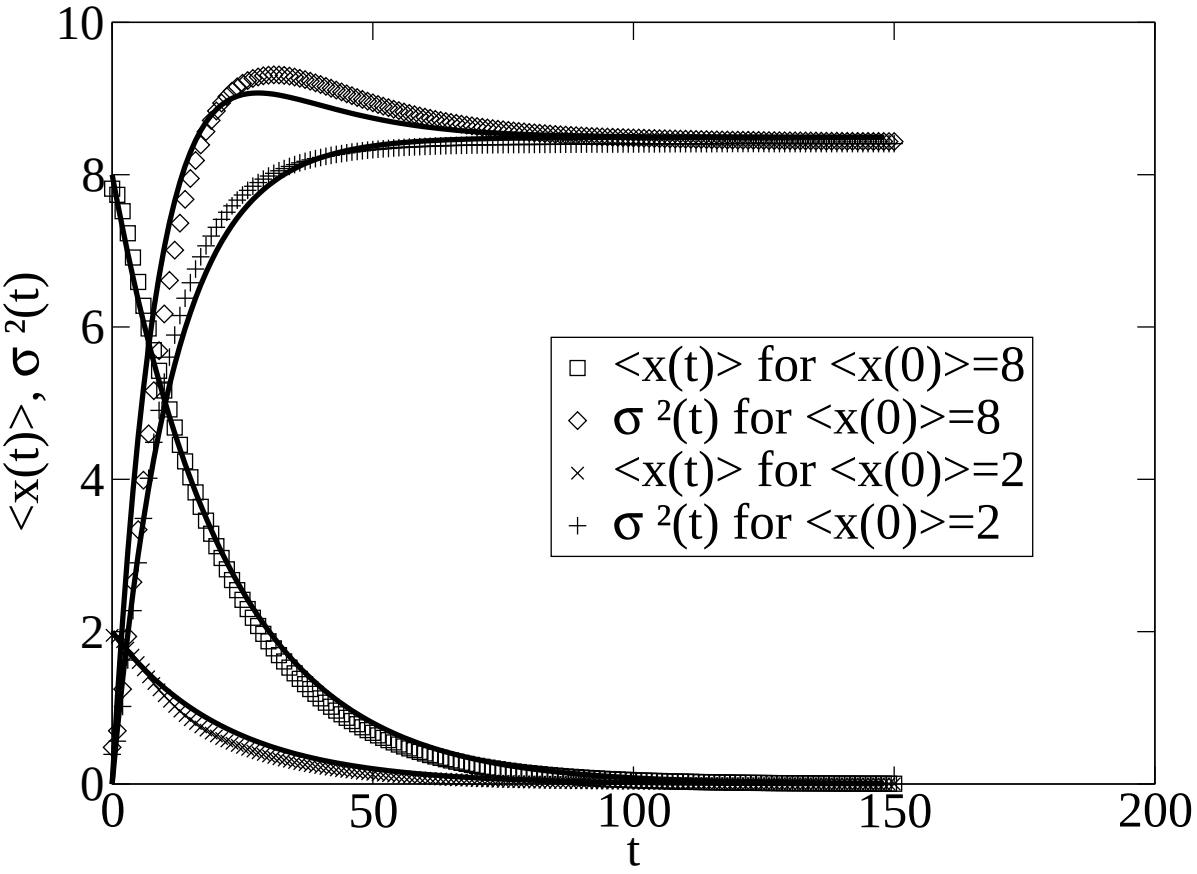

Figure 4.9.: Comparison of the quantum dynamics (markers) for $\langle \hat{x}(t)\rangle$ and $\sigma^2(t)$ for two initial states with $\langle \hat{x}(0)\rangle = 2$ and $\langle \hat{x}(0)\rangle = 8$ for a system consisting of $N = 32$ spins with the dynamics generated from the rate equation mentioned in the text (solid lines)

able agreement indicates that stochastic Markovian dynamics may mimic the coherent quantum dynamics even beyond macroscopic determinism. This is further indicator for thermodynamic behavior in the anisotropic Heisenberg ladder in this parameter and initial state regime.

While the rate equation based on (4.10) and (4.11) can reproduce the quantum dynamics with reasonable agreement even for initial states which are not close to equilibrium,

the question remains whether a stochastic process can be constructed which shares the properties of the above mentioned rate equation, but is not based on ad-hoc assumptions about the rates. A way to do this is to build a discrete Markov chain from the transition probabilities between the magnetization subspaces at certain point in time τ $w_{XY}(\tau)$ which are defined as

$$w_{XY}(\tau) := |\hat{P}_X e^{-i\tau\hat{H}}|\omega_Y\rangle|^2 \tag{4.12}$$

with $|\omega_Y\rangle|$ the initial state starting in magnetization difference subspace Y. If such a description applies the dynamics of the probabilities is given by $P_X(t)$:

$$\vec{P}(n\tau) = W(\tau)^n \vec{P}(0) \tag{4.13}$$

where $\vec{P}(t)$ represents the entity of all $\{P_X(t)\}$ as a vector, and $W(\tau)$ is the transition matrix formed by all $\{w_{XY}(\tau)\}$. From $\vec{P}(t)$ mean and variance may of course be computed as

$$< x(t) >= \vec{X} \cdot \vec{P}(t), \quad \sigma^2 = \vec{X^2}\vec{P}(t) - (\vec{X} \cdot \vec{P}(t))^2 \tag{4.14}$$

where $\vec{X}$ is the vector formed by all $\{X\}$ and $\vec{X^2}$ the vector formed by all $\{X^2\}$. In Fig. 4.10 the dynamics of mean and variance as resulting from the unitary evolution to the dynamics as resulting from (4.12, 4.13) for $\tau = 15$ (this choice is not imperative, however for τ on the timescale of the correlation time the agreement becomes worse) are compared. Obviously, there is reasonable agreement even for states starting far from equilibrium. This indicates that a Markov chain based on $W(\tau)$ may indeed essentially capture the dynamics of the closed quantum system. In order to compare the Markov chain defined by (4.13) to the master equation defined by spin flip model first a matrix of finite transition probabilities $u_{XY}(\tau)$ as resulting from [27] is computed. This is conveniently done numerically. Since it is intended to compare with $w_{XY}(15)$ of course also $u_{XY}(15)$ is computed. In order to be able to compare $w_{XY}(15), u_{XY}(15)$ in an meaningful way matrices a "force" $f(X)$ and a "diffusion coefficient $D(X)$ is assigned to both transition in the following way: The change of the mean $< x(t) >$ during time $t = 15$ given that one started a $< x(0) >= X$ is computed and called $f(X)$. Furthermore, the increase of the variance $\sigma^2(t)$ during time $t = 15$ given that one started a $< x(0) >= X, \sigma^2(0) \approx 0$ is computed and called $D(X)$. Obviously, there is a good agreement for the force (Fig. 4.11(a)) and reasonable agreement for the diffusion coefficient (Fig. 4.11(b)) as calculated form the Markov chain (4.12) and the "naive model" from [27] close to equilibrium ($X = 0$). However, there are also significant differences in the off-equilibrium regime. Based on the numerics at hand any tendency of these differences to vanish in the limit

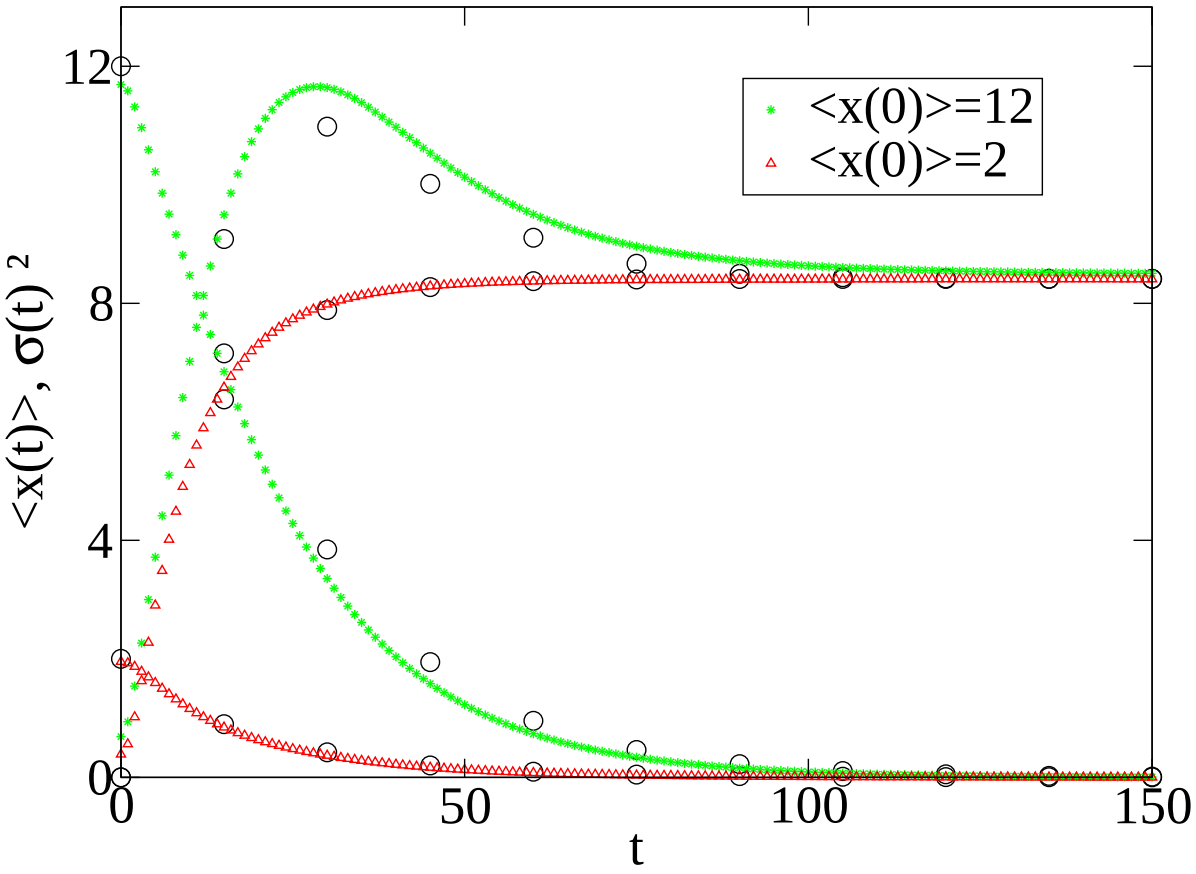

Figure 4.10.: Quantum expectation values $\langle\hat{x}(t)\rangle$ and variances σ^2 of the magnetization difference for $N = 32$ for two states, one starting close to equilibrium $\langle\hat{x}(0)\rangle = 2$ and the other far from equilibrium $\langle\hat{x}(0)\rangle = 12$. Dots represent the corresponding data as calculated from the Markov chain specified by (4.12). This is to be compared with Figs. 4.8 and 4.9. Obviously, the agreement of the quantum dynamics with the respective stochastic model is better here compared to the spin flip model and equally good compared to the model based on (4.10) and (4.11).

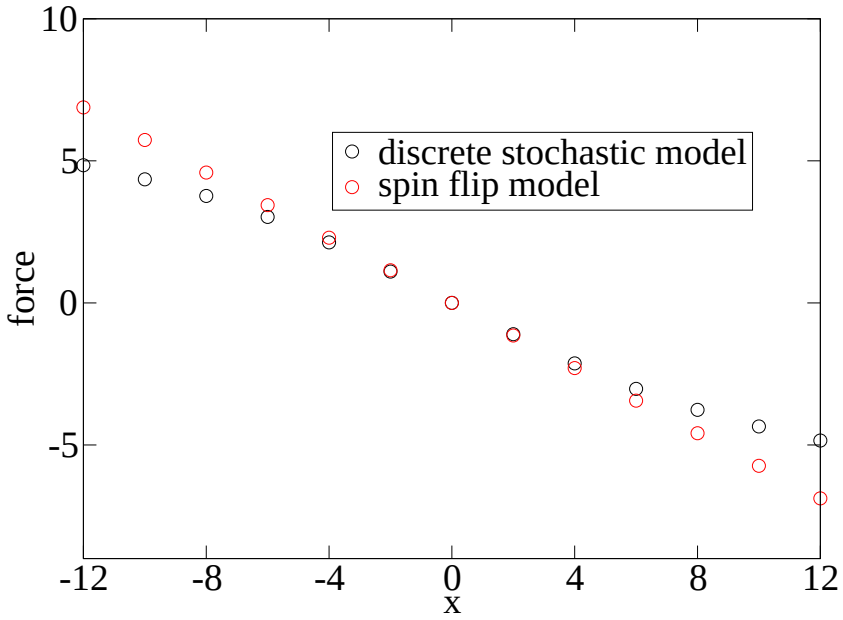

(a)

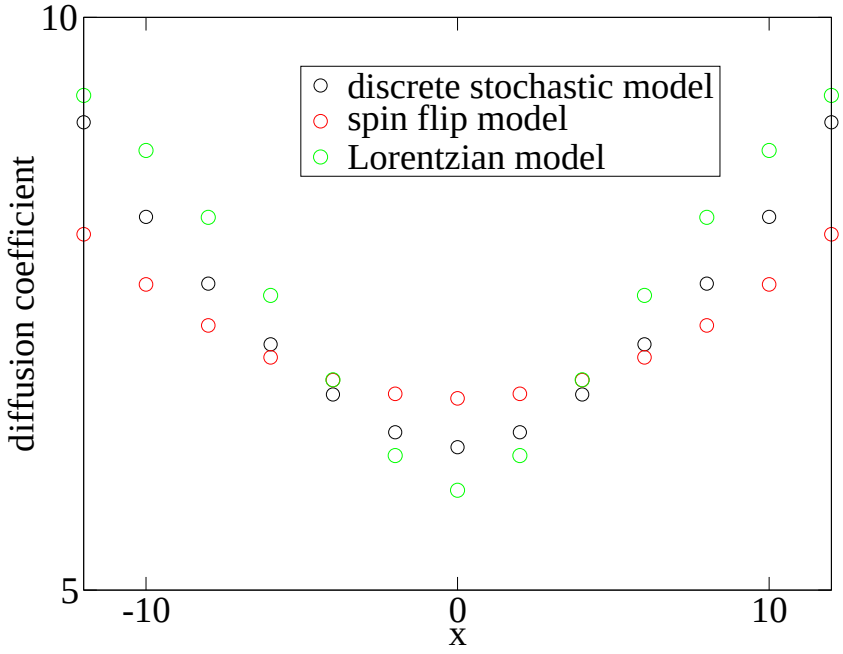

(b)

Figure 4.11.: (a) Quantity corresponding to what would be the force term in a Fokker-Planck equation, calculated for the stochastic models defined by the spin flip model from [27] (which has the same force as the Lorentzian model with the rates described in (4.10) and (4.11)) and the discrete model from (4.12). While the force for the spin flip model is almost strictly linear, the force for (4.12) deviates from that in the off-equilibrium regime. However, the curvature is low on the scale of $\sigma(\approx 3)$. (b) Quantity corresponding to what would be the diffusion term in a Fokker-Planck equation, calculated for the stochastic models defined by the spin flip model from [27], the discrete model from (4.12) and the Lorentzian model from (4.10) and (4.11)) . The diffusion coefficient from (4.12) deviates from the one from the spin flip model in the off-equilibrium regime.

of larger systems cannot be found.

As was demonstrated above the unitary quantum dynamics can be described by a time-continuous Markov chain whose rates are chosen ad-hoc and fitted to the quantum data and a discrete Markov chain with transition probabilities from the actual quantum data. Since both methods yield results with good agreement to the quantum data, it is safe to assume that the dynamics of the anisotropic Heisenberg ladder can be described by a stochastic process which is combined with the results from the previous section a strong indicator for thermodynamic behavior in this closed quantum system.

4.3. Eigenstate thermalization hypothesis

While the eigenstate thermalization hypothesis does not describe the way into equilibrium of a quantum system, it can be a helpful method to describe why a certain final or equilibrium value is reached for the time evolution of an expectation value of a quantum observable independent of the initial state in a certain energy shell. For the dynamics of the anisotropic Heisenberg ladder it was demonstrated that all initial states in a certain energy shell have an expectation value $\langle \hat{x}(t) \rangle$ which relaxes to zero. If large enough systems are chosen ($N = 32$) then this relaxation is Markovian and autonomous and the dynamics of $\sigma(t)^2$ relax towards the typical variance. Thus, this system shows behavior which a quantum system which approximately fulfills the eigenstate thermalization hypothesis for σ^2 and exactly for $\langle \hat{x}(t) \rangle$ would. Therefore, the question whether the eigenstate thermalization hypothesis is responsible for this behavior will be discussed now.

For the time evolution of the expectation value of the magnetization difference $\langle \hat{x}(t) \rangle$ this question can be answered easily: Due to symmetry all eigenstates of the Hamiltonian of the anisotropic Heisenberg ladder $|E_i\rangle$ have

$$\langle E_i | \hat{x} | E_i \rangle = 0 \tag{4.15}$$

and, therefore, the eigenstate thermalization hypothesis is automatically fulfilled for the expectation value of the magnetization difference. Since the non-degeneracy condition of pairs of eigenvalues should be fulfilled for this system, all initial states in all possible

energy shells will have expectation values of the magnetization difference which will relax to zero. This is a valuable insight, but, of course, lacks any knowledge about the dynamics of these expectation values and can only function as addendum to the analysis of the markovicity of the dynamics.

Considering the variance of the magnetization difference $\sigma^2 = \langle \hat{x}^2 \rangle - \langle \hat{x} \rangle^2$, there are no analytic results concerning the eigenstate thermalization hypothesis due to symmetries. But because of (4.15) it is sufficient to consider the eigenstate thermalization hypothesis for $\langle \hat{x}^2 \rangle$. The easiest method to analyze the eigenstate thermalization hypothesis in such a case is to numerically diagonalize the Hamiltonian and compute all expectation values $\langle E_i | \hat{x}^2 | E_i \rangle$. Note that this is only feasible for system up to $N = 16$ spins. In Fig. 4.12 the

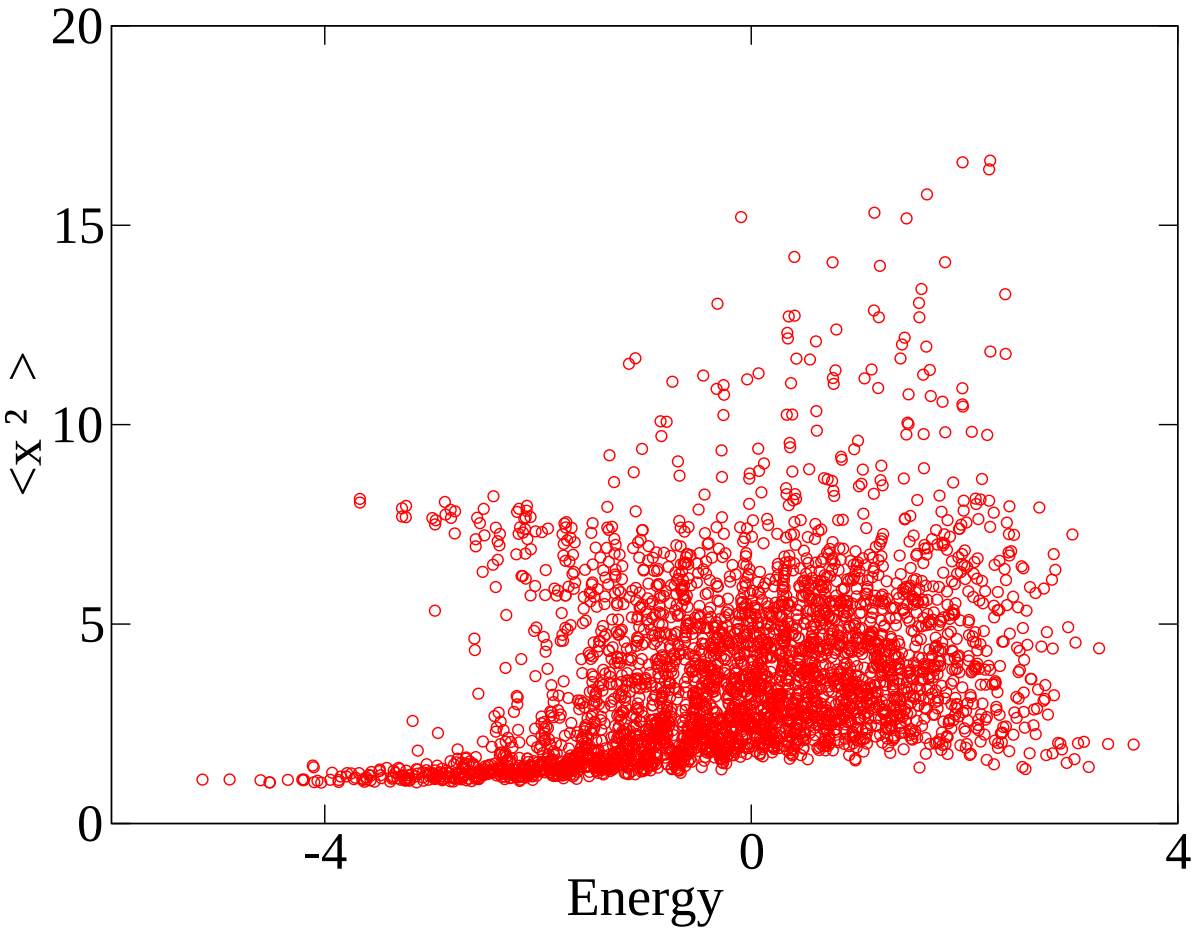

Figure 4.12.: Expectation values $\langle E_i | \hat{x}^2 | E_i \rangle$ for a system of $N = 14$ spins plotted against the corresponding energy eigenvalue E_i. The eigenstates are computed using exact diagonalization.

expectation values $\langle E_i | \hat{x}^2 | E_i \rangle$ are depicted as a function of the energy for a system of $N =$

14 spins whose eigenstates and eigenvalues are computed using exact diagonalization. The spreading of these expectation values is strong and increases with energy. To be able to analyze the amount of spreading of the expectation values $\langle E_i|\hat{x}^2|E_i\rangle$ it is wise to subdivide the energy spectrum in distinct intervals and to calculate the mean of the expectation values $\langle E_i|\hat{x}^2|E_i\rangle$ and its variance Σ^2 for each individual energy interval, which is a quite easy task if all eigenstates and eigenvalues are known. In Fig. 4.13 the

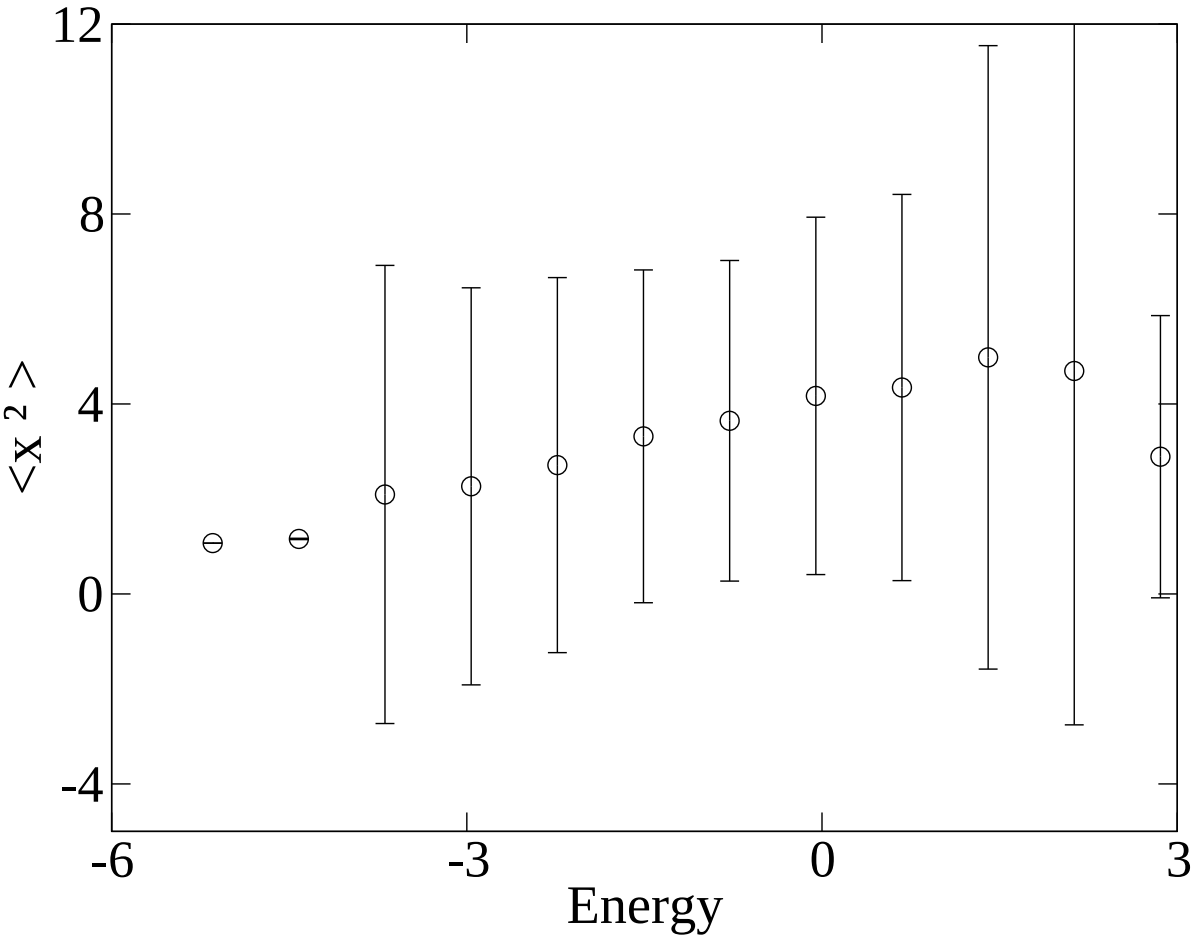

Figure 4.13.: Mean Expectation values of $\langle E_i|\hat{x}^2|E_i\rangle$ and its standard deviation for energy intervals with a width of approximately 0.73 for a system of $N = 14$ spins plotted against the corresponding energy eigenvalue E_i. The eigenstates are computed using exact diagonalization.

same data is used to compute the mean of the expectation values $\langle E_i|\hat{x}^2|E_i\rangle$ and its standard deviation Σ quantifying the strong spreading of the expectation values of the squared magnetization difference. The spreading Σ is an indicator of how different the final variances will be for different initial states within the same energy shell. Since it is known from the numerical computation of the time evolution of the variance of the

magnetization difference σ^2 that the final variances for initial states lie more closely together with increasing system sizes, it is safe to assume that Σ becomes smaller with increasing system sizes at least in the middle of the energy spectrum (only this part was analyzed numerically before for the time evolution of σ^2).

Since large system sizes cannot be diagonalized exactly on reasonable time scales, another method to analyze the eigenstate thermalization hypothesis is needed. A possible way to do this is to compute the mean $\langle E_i|\hat{x}^2|E_i\rangle$ of the variance of the magnetization difference with the eigenstates within a certain energy shell (which is the typical variance $\sigma^2_{\text{typical}}$) and its second moment using typicality and the fourth order Runge-Kutta scheme. The typical variance which is defined in (4.2) and (4.3) is this mean such that only a method for the computation of the second moment Σ^2 of the variance of the magnetization difference with the eigenstates in a certain energy shell needs be developed. The spreading Σ^2 of the expectation values of $\hat{x}^2$ is defined for an energy shell formed by a gaussian filter

$$\Sigma^2 = \sum_n P_n \langle n|\hat{x}^2|n\rangle^2 - \left(\sum_n P_n \langle n|\hat{x}^2|n\rangle\right)^2 \tag{4.16}$$

with $|n\rangle$ the energy eigenstates and $P_n \propto e^{-\alpha/2(E_n-E_f)^2}$ with $\sum\limits_n P_n = 1$. Now it will be demonstrated that pure states drawn from an unitary invariant ensemble can be energy filtered with a Gaussian giving rise to a small Hilbert space variance for systems with a large effective dimension and that they can be used in the computation of Σ^2. The average of the quantum expectation values of a certain observable $\hat{A}$ sampled from these randomly chosen states (which is called the Hilbert space average) and its variance are [11, 49]

$$\text{HA}\left(\langle\psi|\hat{A}|\psi\rangle\right) = \frac{\text{Tr}\left(\hat{A}\right)}{n} \tag{4.17}$$

$$\text{HV}\left(\langle\psi|\hat{A}|\psi\rangle\right) = \frac{1}{n+1}\left(\frac{\text{Tr}\left(\hat{A}^2\right)}{n} - \left(\frac{\text{Tr}\left(\hat{A}\right)}{n}\right)^2\right) \tag{4.18}$$

with n the dimension of the corresponding Hilbert space. For the anisotropic Heisenberg ladder drawing pure states from the unitary invariant ensemble can be achieved by choosing each basis coefficient in the "spin-up/spin-down" basis according to a uniform distribution for the real part and the imaginary part and then normalizing the state.

Introducing the Gaussian energy shift operator (or Gaussian filter)

$$\hat{C} = e^{-1/4\alpha(H-E_f)^2} \tag{4.19}$$

the Hilber space average and variance of the quantity $\theta = n\langle\psi|\hat{C}^2|\psi\rangle$ can be computed

$$\mathrm{HA}\,(\theta) = \mathrm{Tr}\left(\hat{C}^2\right) = \sum_n e^{-1/2\alpha(E_n-E_f)^2} \tag{4.20}$$

$$\mathrm{HV}\,(\theta) = \frac{1}{n+1}\left(n\mathrm{Tr}\left(\hat{C}^4\right) - \mathrm{Tr}\left(\hat{C}^2\right)^2\right) \tag{4.21}$$

with E_n the energy eigenstates of the Hamiltonian and

$$\mathrm{Tr}\left(\hat{C}^4\right) = \sum_n e^{-\alpha(E_n-E_f)^2} \tag{4.22}$$

Assuming that the spectrum of the Hamiltonian is sufficiently smooth at E_f the traces can be approximated by

$$\mathrm{Tr}\left(\hat{C}^2\right) \approx n(E_f)\sqrt{2\pi}\sqrt{\alpha} \tag{4.23}$$

$$\mathrm{Tr}\left(\hat{C}^4\right) \approx n(E_f)\sqrt{\pi}\sqrt{\alpha} \tag{4.24}$$

with $n(E_f)$ the density of states of the Hamiltonian at energy E_f. Introducing the "effective dimension" $d = n(E_f)\sqrt{\alpha}$ the following estimations of the Hilbert space average and variance of θ can be found

$$\mathrm{HV}\,(\theta) < \frac{n}{n+1}\mathrm{Tr}\left(\hat{C}^4\right) < d\sqrt{\pi} \tag{4.25}$$

$$\mathrm{HA}\,(\theta) \approx d\sqrt{2\pi} \tag{4.26}$$

Equation (4.25) means that for a large effective dimension the corresponding Hilbert space variance of θ is small giving rise to a narrow distribution of the Hilbert space average in terms of pure states drawn form an unitary invariant ensemble. This means that $\mathrm{Tr}\left(\hat{C}^2\right)$ can easily be estimated by a small number of randomly chosen pure states and the energy constrained pure state $C/\sqrt{\mathrm{Tr}\left(\hat{C}^2\right)}|\psi\rangle$ can be generated using typicality. Defining the normalized ($\mathrm{Tr}(\rho) = 1$) Gaussian filter operator according

$$\sqrt{\rho} = \frac{\hat{C}}{\mathrm{Tr}\left(\hat{C}^2\right)} \tag{4.27}$$

with this definition the "filter amplitudes" in (4.16) are $\langle n|\rho|n\rangle = P_n$. To calculate the typical variance and to check whether it can be determined from the energy filtered pure states drawn from an unitary invariant ensemble the Hilbert space average and variance of

$$\beta = N\langle\psi|\sqrt{\rho}\hat{x}^2\sqrt{\rho}|\psi\rangle \tag{4.28}$$

Its Hilbert space average is

$$\mathrm{HA}\,(\beta) = \mathrm{Tr}\left(\rho\hat{x}^2\right) = \sum_n P_n\langle n|\hat{x}^2|n\rangle \tag{4.29}$$

which is the typical variance and thus defining a numerical recipe for calculating it using β. From the Hilbert space variance it can now be deduced if the typical variance can be sampled from a view random pure states as was down in the previous sections.

$$\mathrm{HV}\,(\beta) = \frac{1}{N+1}\left(N\mathrm{Tr}\left(\rho\hat{x}^2\rho\hat{x}^2\right) - \left(\mathrm{Tr}\left(\rho\hat{x}^2\right)\right)^2\right) \tag{4.30}$$

The first expression in (4.30) can be simplified further by using $P_k \leq 1/d$

$$\mathrm{Tr}\left(\rho\hat{x}^2\rho\hat{x}^2\right) = \sum P_i\hat{x}^2_{ik}P_k\hat{x}^2_{ki} \leq \frac{1}{d}\sum P_i\hat{x}^2_{ik}\hat{x}^2_{ki} = \frac{1}{d}\mathrm{Tr}\left(\rho\hat{x}^4\right) \tag{4.31}$$

Therefore, the Hilbert space variance of β scales with $1/d$ and for systems with a large effective dimension the typical variance for a Gaussian shaped energy shell $\sigma^2_{\mathrm{typical}} = \sum_n P_n\langle n|\hat{x}^2|n\rangle$ can be computed from a view random drawn, energy filtered pure states. At last the quantity

$$\gamma(t) = N\langle\psi|\sqrt{\rho}\hat{x}^2(t)\hat{x}^2\sqrt{\rho}|\psi\rangle \tag{4.32}$$

has to be analyzed. Assuming that the anisotropic Heisenberg ladder has non-degenerate pairs of eigenvalues averaging over finite time intervals is the same as computing the total time average

$$\overline{\gamma} = \int_{t_1}^{t_2}\gamma(t)\,\mathrm{d}t = N\langle\psi|\sqrt{\rho}\hat{x}^2_D\hat{x}^2\sqrt{\rho}|\psi\rangle \tag{4.33}$$

with $\hat{x}^2_D$ the diagonal representation of $\hat{x}^2$ in the energy eigenbasis. The Hilbert space average of (4.33) is

$$\mathrm{HA}\,(\overline{\gamma}) = \mathrm{Tr}\left(\rho\hat{x}^2_D\hat{x}^2\right) = \mathrm{Tr}\left(\rho\hat{x}^4_D\right) = \sum_n P_n\langle n|\hat{x}^2|n\rangle^2 \tag{4.34}$$

which is the first expression needed for the calculation of Σ^2 (4.16). The definition of $\overline{\gamma}$

is also the numerical recipe for the calculation of this expression: A random state drawn from the unitary invariant ensemble is energy filtered and the operator $\hat{x}^2$ is applied to a copy of it, then both states are evolved in time using an appropriate method and the scalar product between the original state and the copy of it to which again $\hat{x}^2$ is applied to is calculated. The result is then time averaged over an interval in which the dynamic has stopped. If this method is feasible, is again decided by the Hilbert space variance which has the following supremum for $\overline{\gamma}$

$$\mathrm{HV}\left(\overline{\gamma}\right) \leq \frac{1}{d}\mathrm{Tr}\left(\rho\hat{x}_D^2\hat{x}^4\hat{x}_D^2\right) \tag{4.35}$$

which again scales with the inverse effective dimension making this method good for the systems at hand. This method is much faster compared to exact diagonalization and its only sources of error are introduced by the statistical error due to the random drawing of the initial states and the approximation of the time evolution by the Runge-Kutta scheme. In order to estimate t_1 and t_2 in (4.33) $\gamma(t)$ is calculated and the values are chosen manually from the resulting curve to enclose an interval in which $\gamma(t)$ shows no dynamics apart from oscillations (Fig. 4.14). Figure 4.15 shows the results of this method for a system of $N = 14$ spins compared to the exact diagonalization results. The results for the typical variances $\sigma^2_{\mathrm{typical}}$ and its spreading Σ as a function of the energy are approximately the same. The main disadvantage of the Runge-Kutta method of estimating the eigenstate thermalization hypothesis becomes visible in this figure: It cannot be used in regions of the Hilbert space where only a few energy eigenstates are because the state $|\psi\rangle$ cannot be constrained to these energy regions without high statistical errors due to the low effective dimension at the edges of the spectrum.

In Fig. 4.16 the typical variance and its spreading are depicted for $N = 20$ with calculations based on typicality and the fourth order Runge-Kutta scheme. While the dependency of the typical variance on the energy stays roughly the same, the spreading of variances within the energy intervals has decreased strongly. The decrease in the spreading Σ indicates that the eigenstate thermalization hypothesis plays a role in the thermalization process of this quantum system by ensuring that even for different initial states the equilibrium state is the same. In Fig. 4.17 the ratio $\sigma^2_{\mathrm{typical}}/\Sigma$ is depicted as a function of the energy for certain system sizes. It can be seen that for all energy intervals the ratio $\sigma^2_{\mathrm{typical}}/\Sigma$ becomes smaller meaning that the relative spread of the expectation values of $\hat{x}^2$ becomes smaller for larger systems regardless of the energy shell.

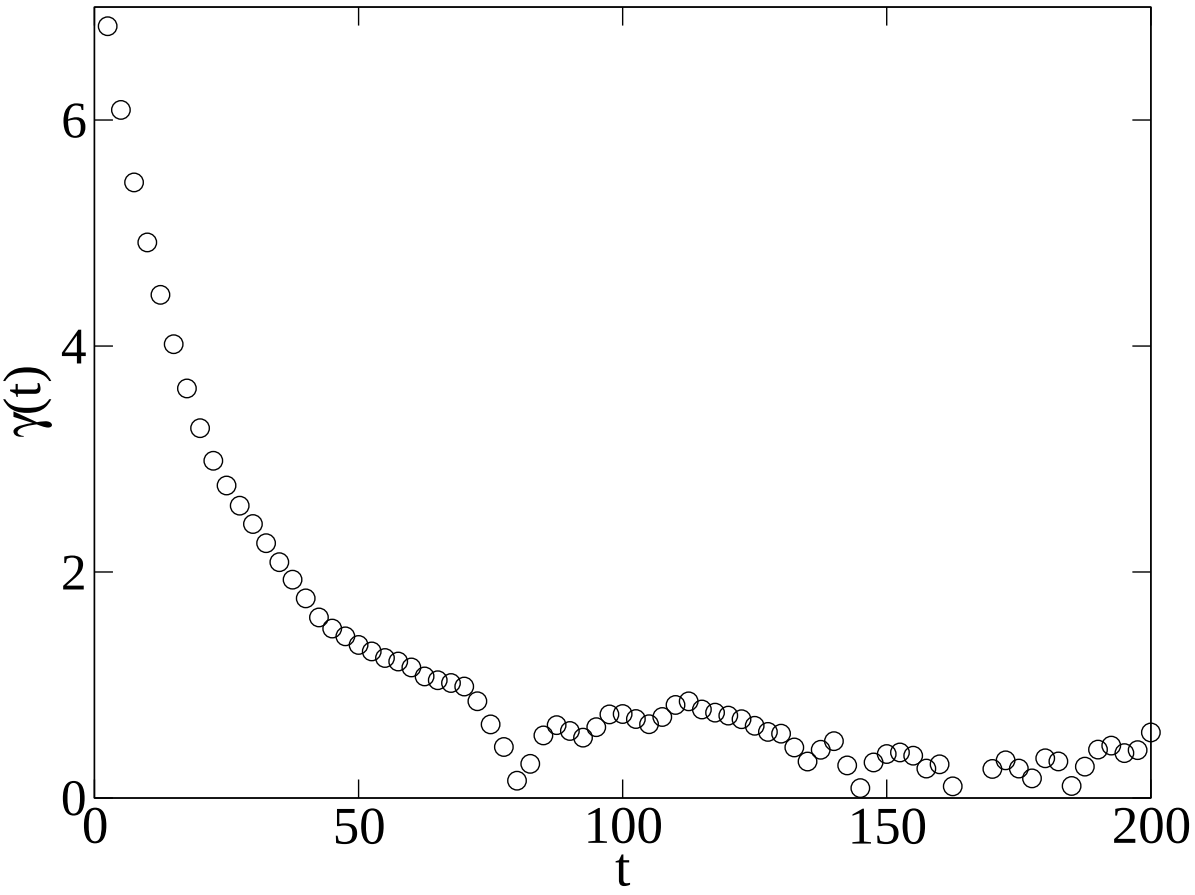

Figure 4.14.: The property $\gamma(t)$ as a function of time for a system comprising 20 spins and $U = 0$. The relaxation dynamics yield after $t \approx 150$ indicating possible choices for t_1, t_2 in (4.33)

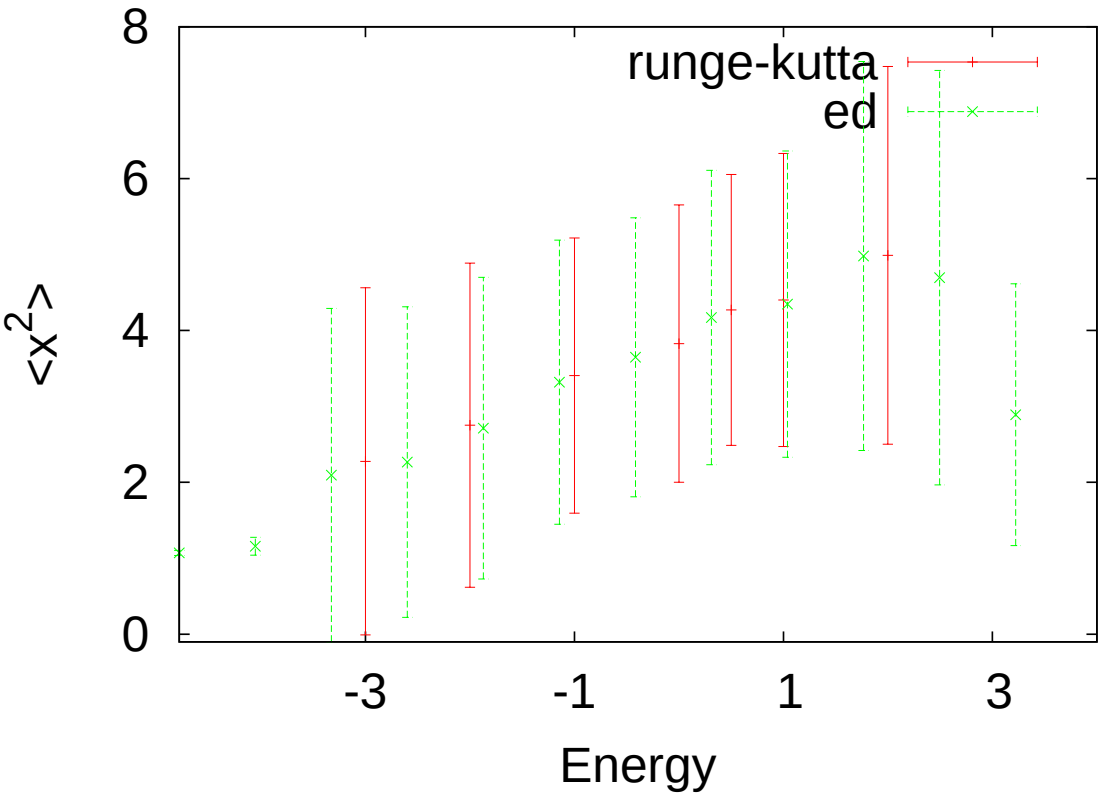

Figure 4.15.: Typical variance $\sigma^2_{\text{typical}}$ of the magnetization difference and its standard deviation Σ regarding the variances of the magnetization difference of the energy eigenstates in the corresponding energy shell for energy intervals with a width of approximately 0.73 for a system of $N = 14$ spins plotted against the corresponding energy. Both exact diagonalization and the Runge-Kutta scheme are depicted.

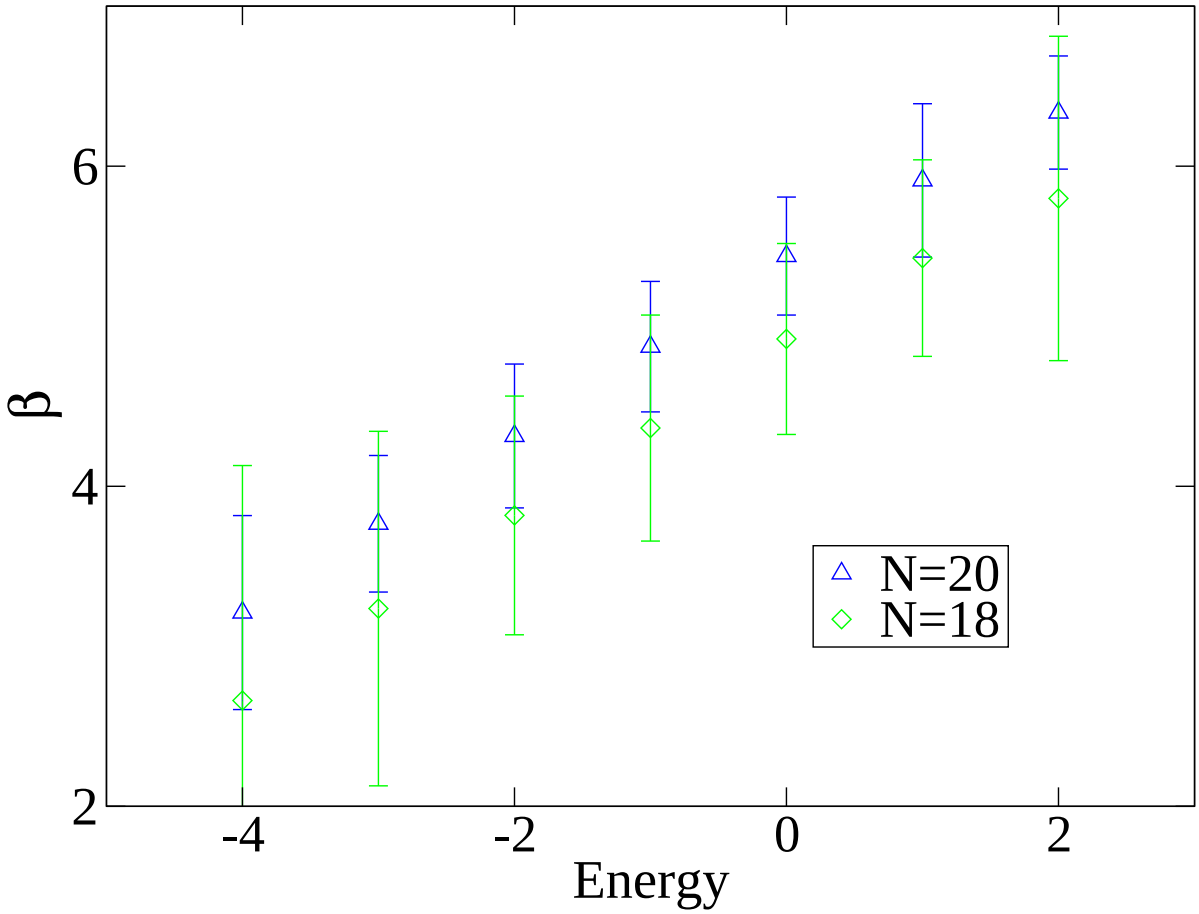

Figure 4.16.: Typical variance $\sigma^2_{\text{typical}}$ of the magnetization difference and its standard deviation Σ regarding the variances of the magnetization difference of the energy eigenstates in the corresponding energy shell for energy intervals with a width of approximately 0.73 for systems of $N = 20$ and $N = 24$ spins plotted against the corresponding energy. Calculations for this data were performed using the Runge-Kutta-scheme.

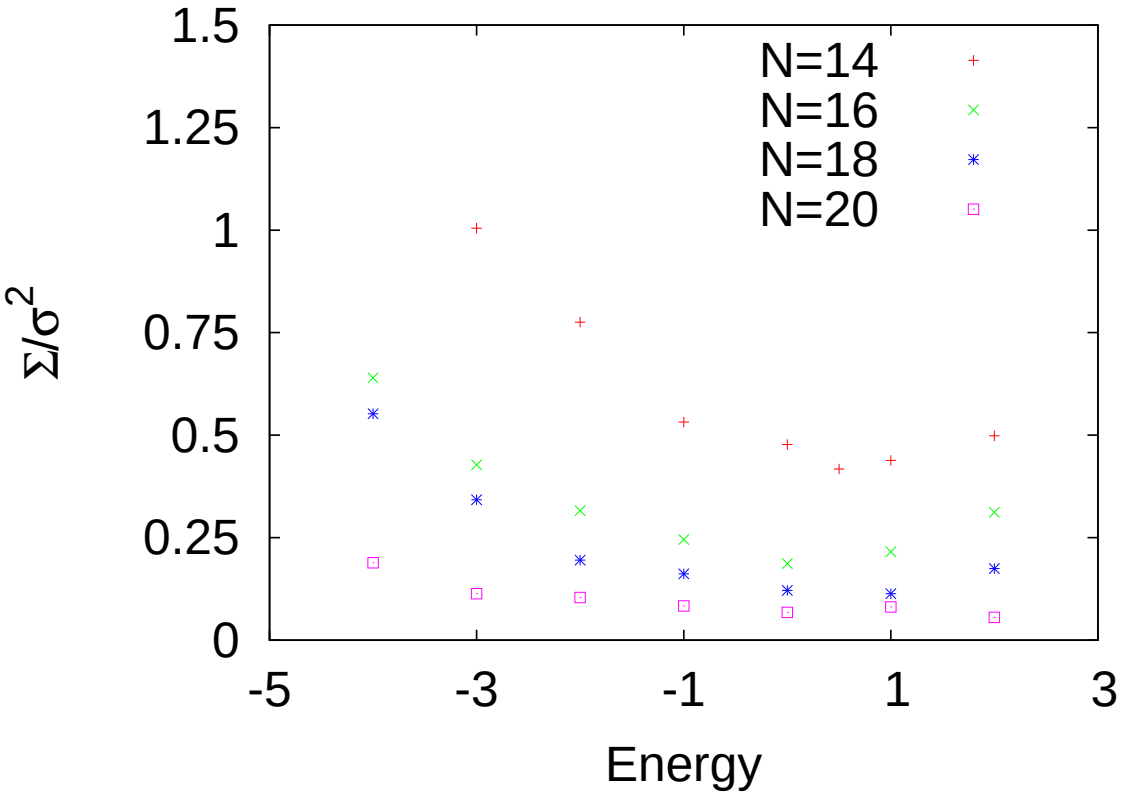

Figure 4.17.: The ratio of the spreading Σ of variances of magnetization difference in a certain energy shell to the typical variance $\sigma^2_{\text{typical}}$ in the same energy shell plotted against the energy for different system sizes.

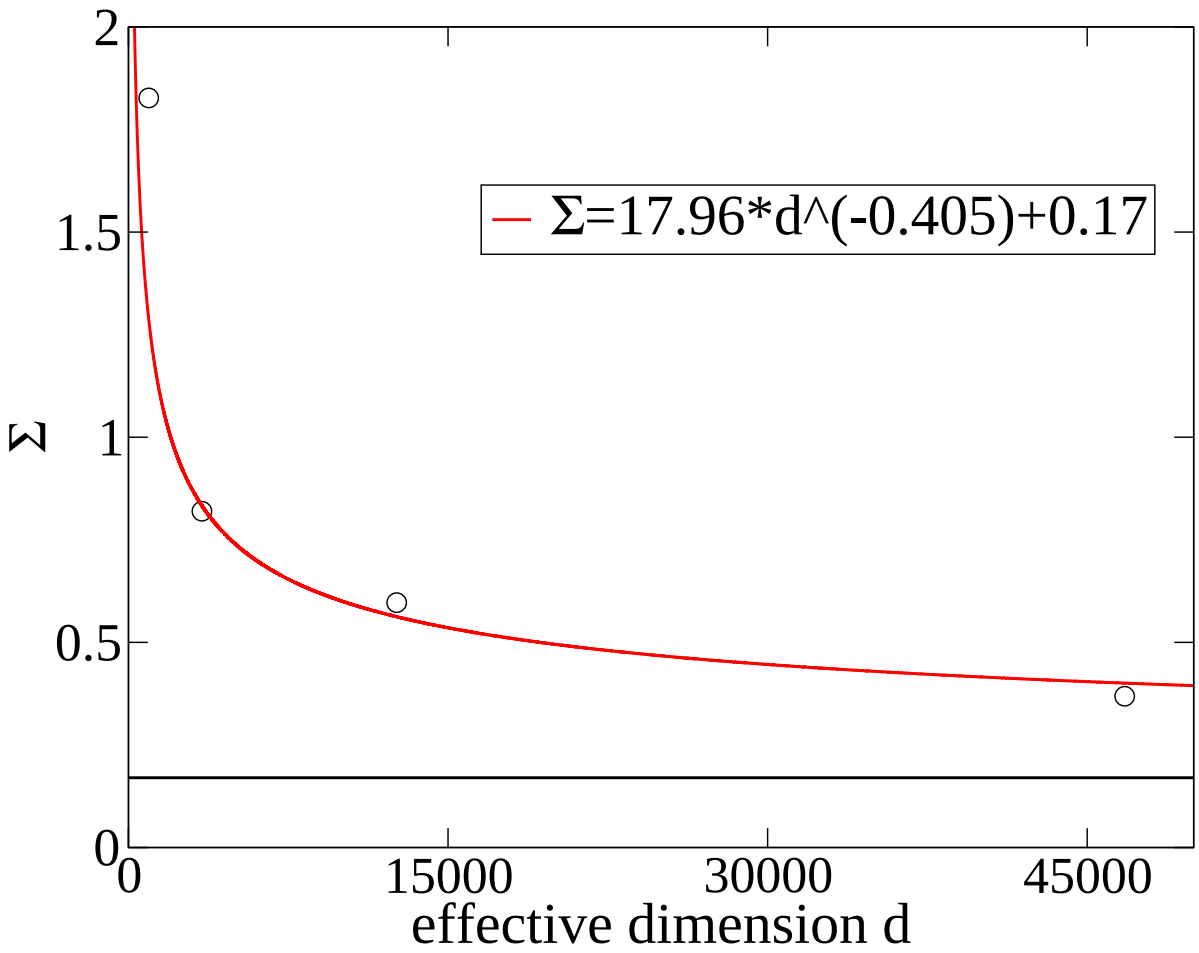

Figure 4.18.: The spreading of the quantum expectation values of $\hat{x}^2$ with the energy eigenstates Σ as a function of the effective dimension of the energy filtered subspace sampled from 10 states drawn at random from the unitary invariant ensemble for $E_f = 0$. The red curve represents a power law fit with an offset $\Sigma(N = \infty) = 0.17$ corresponding to the finite width of the energy subspace (see text). The straight black line is this offset.

The eigenstate thermalization hypothesis is fulfilled if in the limit of large systems and small energy subspaces $N \to \infty$ and $\mathrm{Var}\left(\hat{H}\right) \to 0$ the spreading vanishes $\Sigma \to 0$. Due to the large computational effort needed to achieve very small energy subspaces the second limit is omitted and the scaling of Σ with the dimension only is analyzed. Because of the finite energy width it is clear that Σ cannot decrease to zero even in the limit of large systems, but will reach an offset $\Sigma(N = \infty)$ which is determined by the slope of $\beta(E)$ over the energy subspace. It can be calculated by approximating $\beta(E)$ by a linear function using a fit and calculating its standard deviation with the normal distribution formed by the Gaussian energy filter. This analysis is depicted in Fig. 4.18 for a systems comprising $14, 16, 18, 20$ spins and the chosen energy subspace centered around $E_f = 0$: There Σ is plotted against the effective dimension d which is defined in (4.23). The effective dimension is a technical byproduct of the normalization of the random pure state drawn from the unitary invariant ensemble with a Gaussian filter and represents the number of states in the actual energy subspace. In case that the density of states does not change its shape, if the system size is increased, the effective dimension is merely a fraction of the complete dimension of the Hilbert space considered regardless of system size. The results from Fig. 4.18 show that $\Sigma(d)$ can be described by a power law with the offset calculated with the above mentioned method indicating that this system might fulfill the eigenstate thermalization hypothesis.

5. Consistent histories and Markovian quantum dynamics

In the last chapters the thermalization process of a spin ladder and the similarities of this process to a classical master equation were discussed. Since dynamics of quantum expectations values the anisotropic Heisenberg ladder can be described by a Pauli master equation, it remains an interesting question whether the dynamics of quantum systems can be treated as a stochastic process on the level of projective measurements.

A way to answer this question is to assign a probability to a list of consecutive, projective measurements performed on a quantum systems using the "consistent history formalism" (which is always possible but does not yield results in accordance with the laws of probability for all systems) and check whether these assigned probabilities are Markovian in the sense that the outcome of the next measurement depends only on the last one and not more or even all measurements already performed on the system.

5.1. Consistent history formalism

So far the dynamics of the quantum systems considered have been entirely treated like classical, Markovian, stochastic processes on the space of distinguishable mesostates because of the similarities of their dynamics with Pauli master equations. However, such an interpretation (even without the "Markovian") is not necessarily in accord with quantum mechanics on the level of measurements. The prime example is the double slit experiment: The probability of the particle to hit the screen at a certain point simply cannot be expressed as the sum of the probabilities of the particle passing through either slit and then proceeding to the above point, i.e., the sum rule of probabilities is

not fulfilled. Hence for the double slit experiment the quantum histories of the particle w.r.t. to its positions are not consistent or "decoherent" (cf. formal definition below). However quantum histories of other systems with respect to other "propositions" may be consistent, i.e., fulfill the sum rule. The latter is an indispensable prerequisite for the description of the quantum dynamics of the systems at hand w.r.t. the mesostates in terms of a master equation and the unraveling of its solution in terms of stochastic trajectories. The mere existence of the concept of a Pauli master equation suggests such a consistency, however, the derivation of the Pauli master equation and a precise formulation of its limits of applicability is somewhat subtle [4, 50, 51, 52, 53]. It should also be mentioned here that a valid derivation of a Pauli master equation on the basis of projection operator techniques does not yet sufficiently proof consistency since it does not directly allow for the calculation of the probability of a quantum history (comprising more than one event). The question of consistency in non-equilibrium quantum systems has been addressed in literature quite frequently, e.g., [54, 55], for an overview see [56], however, these investigations address specifically consistency of position measurements in systems of the Caldeira-Legett-type, which are all open quantum systems.

Also somehow implied by a Pauli master equation description, but different from consistency is Markovicity. Here we call a quantum history or sequence of events Markovian if its probability may essentially be written as a product of the probabilities of subsequent events. This is of course only possible if the probability of any event exclusively depends on the previous event.

In the remainder of this section we give some more concrete specifications of consistency and Markovicity and introduce a non-specific and rather simple Hamiltonian model tailored to facilitate a numerical check of consistency and Markovicity. This check will be restricted to some somewhat arbitrary examples and is more intended to be a proof of principle rather than an exhaustive detailed analysis.

A quantum history is a list of events (results of measurements) on a quantum system which is assigned a probability through the consistent history formalism as developed by Griffith, Omnes, Gell-Mann, Hartle and others [57, 58, 59]. The events are represented by consecutive (not necessarily but often) projective measurements on the time-evolving quantum system. For example, consider a quantum system which is in the state ρ at $t = 0$, then a measurement is performed on the system yielding the property represented by the projector $\hat{P}_{\alpha_1}$ at time t_1, then at t_2 the property $\hat{P}_{\alpha_2}$ is measured and so on.

Thus, the the history operator C_α with α the set of different projective measurements is defined as

$$\hat{C}_\alpha = \ldots \hat{P}_{\alpha_2} e^{-iH(t_2-t_1)} \hat{P}_{\alpha_1} e^{-iHt_1} \tag{5.1}$$

with $\alpha_1, \alpha_2, \ldots \in \alpha$ and $\sum\limits_n P_{\alpha_n} = 1$. Intuitively, one would assign the probability $p_\alpha = \mathrm{Tr}\left(\hat{C}_\alpha \rho \hat{C}_\alpha^\dagger\right)$ to the history $\hat{C}_\alpha$. For this to be true, the so assigned probabilities must fulfill the axioms of probability meaning they have to be non-negative, normalized and the sum rule of probabilities (the third axiom of Kolmogorov which states that the sum of all possible probabilities is one) must apply. It can easily be seen that the so assigned probabilities are non-negative and normalized, but what about the sum rule? It states that probabilities are additive for disjoint events. That this needs not to be true can be seen if unity is inserted into the expression for the probability of measuring $\hat{P}_{\alpha_2}$ at $t = t_2$ in the Heisenberg picture.

$$\mathrm{Tr}\left(\hat{P}_{\alpha_2}(t_2)\rho\hat{P}^\dagger_{\alpha_2}(t_2)\right) = \sum_{\alpha_1,\alpha_1'} \mathrm{Tr}\left(\hat{P}_{\alpha_2}(t_2)\hat{P}_{\alpha_1}(t_1)\rho\hat{P}^\dagger_{\alpha_1'}(t_1)\hat{P}^\dagger_{\alpha_2}(t_2)\right) \tag{5.2}$$

In (5.2), there are more summands than just the probabilities of all possible histories. In addition to the history probabilities, there are terms with different histories on the left and on the right of the density operator in the trace. These inconsistency or decoherence terms must vanish in order for the histories obeying the sum rule of probabilities meaning

$$\mathrm{Tr}\left(\hat{C}_\alpha \rho \hat{C}_\beta\right) = 0 \tag{5.3}$$

for all possible pairs of different histories which the system may undergo. If this is true, the measurement can be considered purely classical since the occurrence of the measurement have any influence at all on the system. There are two possible explanations for the fact that (5.3) is true in some quantum systems: If the measurement device itself is a part of the quantum system, it can play a vial part in the decoherence of the quantum mechanics leading to (5.3) to be true (an example for this is the double slit), but there are also systems for which (5.3) is true without explicitly incorporating the measurement device, which is what is aimed for here.

Our model quantum system consists of two identical subunits with n states and bandwidth $\delta\epsilon$, which are coupled with the average interaction strength λ.

$$H = \sum_{i=0}^{n-1} \frac{i}{n-1}\delta\epsilon|i\rangle\langle i| + \sum_{j=0}^{n-1} \frac{j}{n-1}\delta\epsilon|j\rangle\langle j| + \sum_{i,j=0}^{n-1} \lambda \cdot e^{i\theta_{ij}}|i\rangle\langle j| \tag{5.4}$$

with θ_{ij} being uniformly distributed random numbers in the interval $[0; 2\pi]$ so that every element of the coupling matrix has the amplitude λ, but the phases are randomly distributed. For simplicity, the density of states in both subunits are the same. This system type has been analyzed before, see, e.g., [53, 60] and obeys a classic rate equation with rates according to Fermi's golden rule (relaxation time $\tau_R = 1/(2\pi\lambda^2 n/\delta\epsilon)$ if the conditions $2\lambda n/\delta\epsilon \geq 1$ and $\lambda^2 n/\delta\epsilon^2 << 1$ are fulfilled (Fig. 5.1), which essentially boils down to the correlation time $\tau_C = 2\pi n/\delta\epsilon$ being small to the relaxation time as mentioned above.

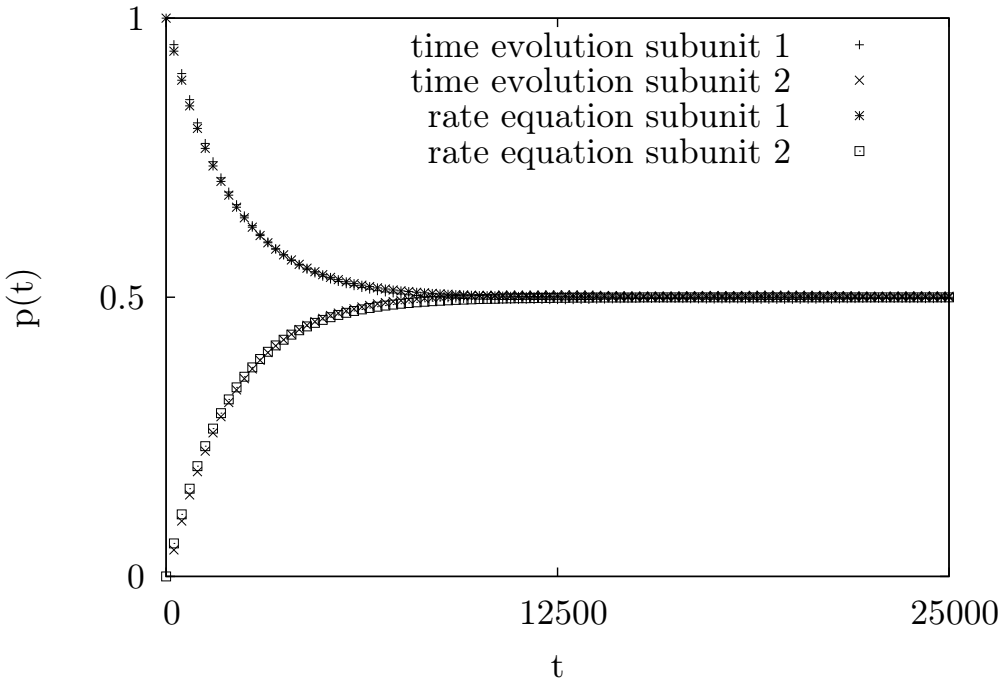

Figure 5.1.: A plot of the comparison of probability of being in the first $p_1(t) = \langle \hat{P}_1(t) \rangle$ or second subunit $p_2(t) = \langle \hat{P}_2(t) \rangle$ of a two part system calculated by exact diagonalization of the Hamiltonian mentioned in the text with the solution of the corresponding classical rate equation for $n = 800$, $\lambda = 5 \cdot 10^{-5}$ and $\delta\epsilon = 0.05$ yielding $\tau_R = 3979$ and $\tau_C = 126$ (see [53] for details). The exact probabilities are calculated using the time-evolution of a completely mixed state in the first subunit. The rate equation and the exact probabilities agree very well.

For the consistency check we choose to consider a set of histories in which the system is in a completely mixed state in the first subunit at $t = 0$, then at time $t = \Delta t$ a measurement is performed on the system finding the system either in the first or second subsystem and, finally, at time $t = 2\Delta t$ the system is found in the second subunit through

a measurement. This setup is essentially (5.2). We subtract the sum of the probabilities corresponding to the two possible histories from the total transition probability from the first to the second subunit during time $t = 2\Delta t$, thus finding the magnitude of the inconsistencies which we divide by the probability of finding the system in the second subunit at time $t = 2\Delta t$ so that a small number indicates consistent histories. Note that this criterion not directly verifies (5.3), but rather checks whether

$$\sum_{\alpha \neq \beta} \mathrm{Tr}\left(\hat{C}_\alpha \rho \hat{C}_\beta\right) = 0 \tag{5.5}$$

which is weaker than (5.3), but it seems rather unlikely that the terms in (5.5) all cancel each other out but are very large the same time. As can be seen in Fig. 5.2 the histories

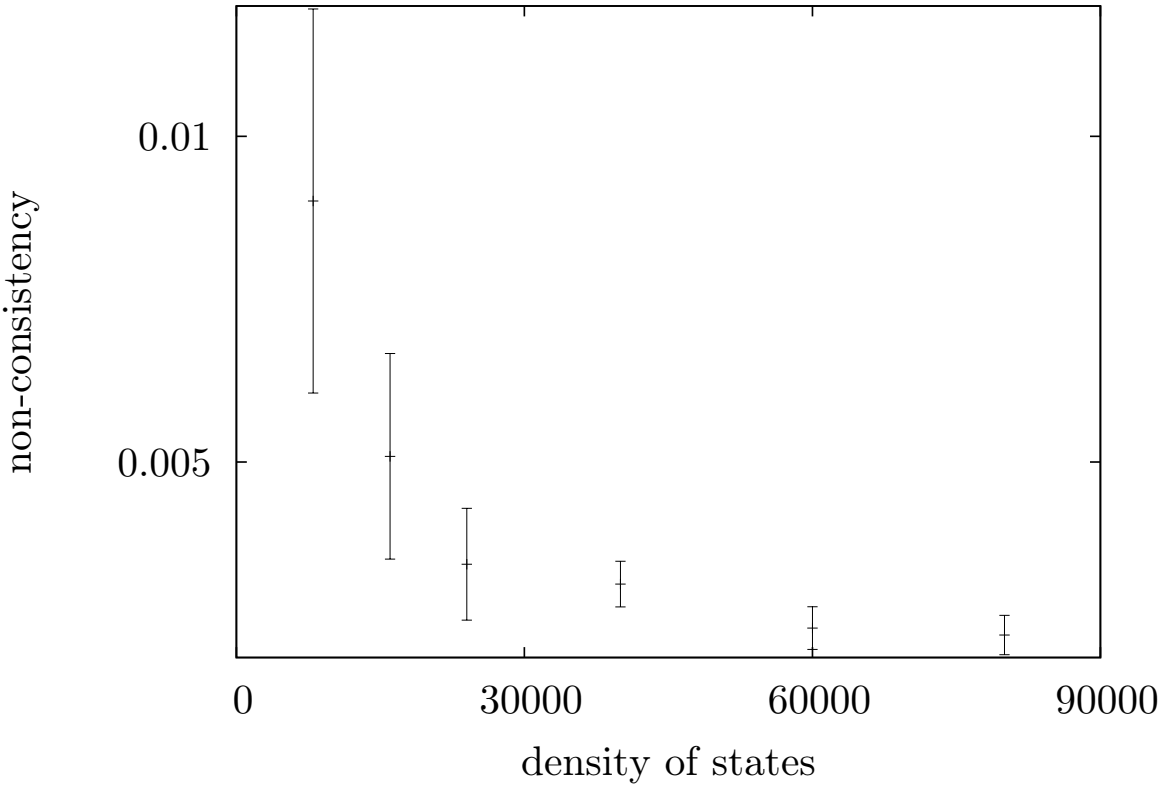

Figure 5.2.: A plot of the consistency check as described in the text versus the density of states $n/\delta\epsilon$ for a system consisting of two subunits for $\delta\epsilon = 0.05$, $\tau_R = 3979$, $\Delta t = \tau_R$ and $\tau_C = 126$. The error bars are generated by checking the consistency criterion for different realizations of the Hamiltonian mentioned above and then estimating mean and variance. With growing density of states the inconsistencies vanish and the single quantum histories can be assigned meaningful probabilities.

become more consistent for higher density of states and in the limit $n/\delta\epsilon \to \infty$ the inconsistency terms vanish thus allowing the mapping of the quantum system onto a stochastic process as done in the previous sections.

The question remains whether the dynamics of this system are also Markovian. The possibility to describe the probabilities of being in either one of the subsystems by a classical rate equation as seen in Fig. 5.1 points in that direction. The previous analysis of this model in also points in that direction but is not conclusive in general since this analysis relies on a projection operator method which can only model the first step in every history of the mixed ρ at $t = 0$ to the first measurement since after the measurement the "new initial state" is not completely mixed anymore and cannot be used in the projection operator method, which neglects an inhomogeneity of a, e.g., Nakajima-Zwanzig equation. Therefore, we numerically analyze if the system shows Markovian dynamics be comparing probabilities generated by the consistent histories formalism to probabilities resulting from splitting the history into pairs of conditional transition probabilities. For example, if the system is Markovian the following identity would be true if we consider the same setup as in the consistency check

$$\mathrm{Tr}\left(\hat{P}_2(t_2)\hat{P}_1(t_1)\frac{\hat{P}_1(0)}{n}\hat{P}_1^\dagger(t_1)\hat{P}_2^\dagger(t_2)\right) = \mathrm{Tr}\left(\hat{P}_2(t_2)\frac{\hat{P_1(t_1)}}{n}\hat{P}_2^\dagger(t_2)\right)\cdot\mathrm{Tr}\left(\hat{P}_1(t_1)\frac{\hat{P}_1(0)}{n}\hat{P}_1^\dagger(t_1)\right) \tag{5.6}$$

meaning that a history can be split up into a sequence of conditional probabilities of pairs of transitions. In (5.6) the particle starts in subsystem 1, is then measured there at time t_1 and is measured in subsystem 2 at time t_2. For our analysis we choose again a system starting completely mixed in the first subsystem, measure once in between at $t = \Delta t$ and end up in subsystem two at $t = 2\Delta t$. As a criterion for being Markovian we calculate the difference between the history probability from the consistent history formalism (left side of (5.6)) and the probability which the Markovian assumptions assigns to the history (right side of (5.6)). The absolute value of the difference is divided by the consistent history formalism probability (left side of (5.6)) and, thus, a small number indicates that the system tends to be more Markovian.

Fig. 5.3 shows the results of this analysis: Like with the consistency discussed above in the limit $n/\delta\epsilon \to \infty$ the system becomes Markovian, thus, justifying all the statements about rate equations for quantum systems made in the previous sections. Note that the densities of states discussed for the consistency and Markovian check are still pretty small

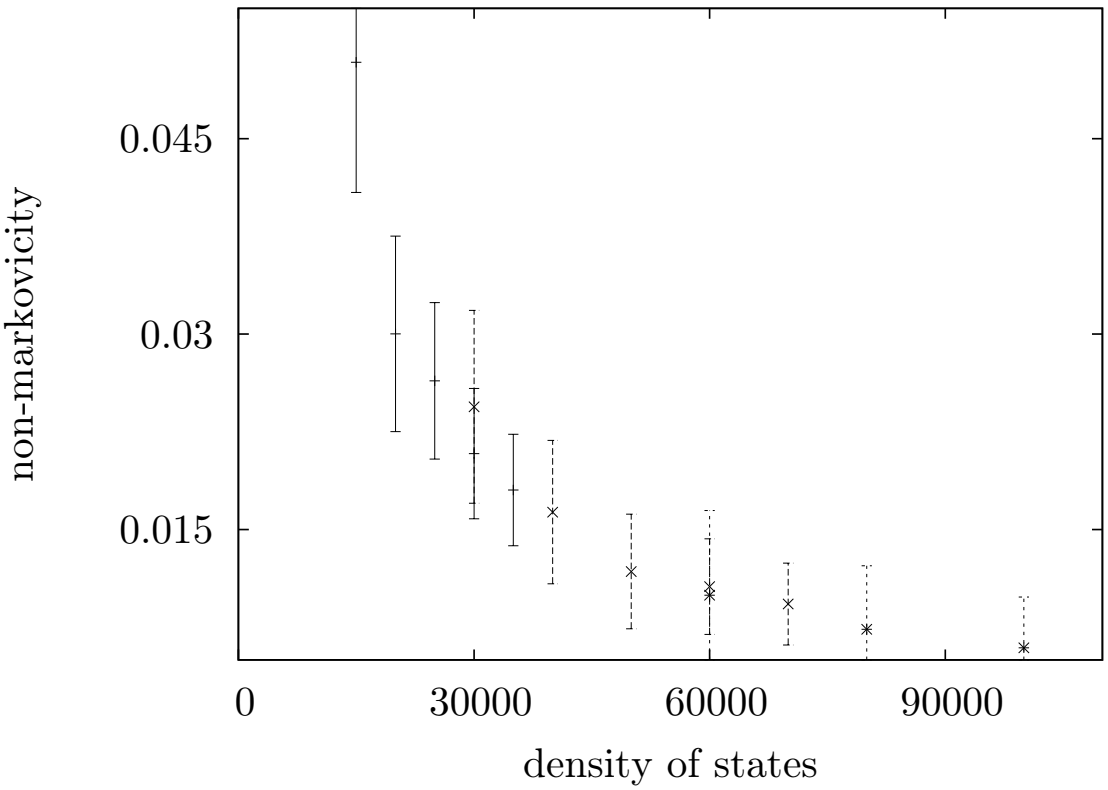

Figure 5.3.: A plot of the Markovian criterion as described in the text versus the density of states $n/\delta\epsilon$ for $\Delta t = \tau_R$. Three systems with $\delta\epsilon = 0.1$ (+),$\delta\epsilon = 0.05$ (x) and $\delta\epsilon = 0.025$ (*) where used while all other parameters and the method of generating error bars were chosen as in Fig. 5.2. In the limit of large densities of states of the system the Markovian criterion approaches zero and, thus, it is safe to assume that the system has Markovian dynamics.

compared to macroscopic systems so that for a real macroscopic system the criterions would be indistinguishable from zero.

6. Conclusion

In this thesis a medium sized, closed, quantum spin system modeled after a signature setup in non-equilibrium thermodynamics, namely a hot and a cold body which are in contact with each other, was analyzed for signs of thermodynamic behavior. These signature signs of thermodynamic behavior were adopted from the macroscopic observation of non-equilibrium thermodynamics:

- **Unique Equilibration**: Thermodynamic observables like the temperature difference have an autonomous and Markovian relaxation process free of memory effects, which means that the relaxation itself does not depend on the initial state of the system and an unique equilibrium is reached.

- **Autonomy**: The statistical variance of the observed quantity is negligible compared to the order of magnitude of the observable meaning that, if two equal systems of such kind are prepared in the same initial state, their relaxation process is indistinguishable.

- **Stochasticity**: The relaxation process can be described by a Pauli master equation of the Fokker-Planck type for the individual measuring values.

While for the macroscopic world it is clear that these "thermodynamic axioms" are fulfilled, the question whether and how a small quantum system on the order of magnitude of a molecule would behave was unclear. The data presented in this thesis shows that the anisotropic Heisenberg ladder shows these signature signs of thermodynamic behavior for the magnetization difference between the beams of the ladder even for a medium sized (32 spins) system with a large improvement compared to small system comprising 16 spins. Although this was only checked for a certain setup of geometry of the spins and parameters, there is hope that these findings can be reproduced for other systems on a

similar order of magnitude concerning the system size, which is still very tiny compared to the macroscopic world but this remains subject to further research. Furthermore, other forms of initial states remain also a valid question for future research: The initial states used throughout this thesis were centered at energy $E = 0$ where the density of states is highest and the fulfillment of the eigenstate thermalization hypothesis is best, but this scenario represents in terms of thermodynamics an infinite temperature. Whether initial states with "finite temperature" in terms of Gaussian filtered pure states with a small variance in energy space but centered at a different energy or pure states resembling a Gibbs state will also show signature signs of thermodynamic behavior in this quality, needs to be analyzed in the future.

The numerical methods used in this thesis, namely the use of randomly drawn pure states from an unitary invariant ensemble, which are then constrained to an energy shell using a Gaussian filter, also provide a case study to the usefulness of methods from solving systems of ordinary differential equations in quantum mechanics: It was demonstrated and proven using typicality that initial pure states constrained to an energy shell can be constructed from the unitary invariant ensemble with little effort and that the numerical computation of this energy filter can be achieved with little error. Furthermore, quantum expectation value as a function of time can be reliably computed using the Runge-Kutta or Chebyshev expansion. Using this findings, a numerical method to check the eigenstate thermalization hypothesis was developed: While usually the corresponding Hamiltonian is diagonalized and quantum expectation values of certain observables of interest for energy eigenstates are computed, this method does not rely on the knowledge of the exact energy eigenstates. Using only the ability to generate typical energy filtered pure states and calculate their time evolution, the (Gaussian weighted) average of quantum expectation values with the energy eigenstates and their respective variance. This method was utilized to check the eigenstate thermalization hypothesis for the anisotropic Heisenberg ladder and the fulfillment of the ETH was identified as the cause of the relaxation of the magnetization difference and its variance towards an unique equilibrium value.

At last it was analyzed whether markovicity can also be found on the level of sequences of measurements on a quantum system: The consistent history formalism provides an interpretation of quantum mechanics in which sequences of measurements or quantum histories can be assigned a probability. These probabilities need not abide to the classical laws of probability, but it was demonstrated that for a simple quantum system with a

random Hamiltonian this is the case and in the limit of large systems these histories become Markovian.

All in all, it could be demonstrated that closed quantum systems can show signature signs of thermodynamic behavior without modifying the standard Schroedinger equation or any other further constraints related to standard quantum mechanics. Furthermore, the eigenstate thermalization hypothesis was identified as the leading factor in the development of the unique equilibrium value, which is independent of the chosen excitation from equilibrium in this system.

A. Source Code

In this chapter the C++ source code to initialize the Hamiltonian for the ansisotropic spin ladder and how to solve it using sparse matrices and the fourth order Runge-Kutta method will be discussed. As a library for sparse matrices and their linear algebra operations the open source version of the matrix template library [37] is used.

At first a list of all basis states in the "spin-up spin-down" representation in the subspace with total magnetization zero is generated by building all possible permutations of $(11111\ldots10000\ldots)$ with $N/2$ spin-ups (represented by 1 internally) and $N/2$ spin-downs (represented by 0)

```
void copy_state_from_into(int* original, int* copy, const int N)
        {
        for(int i = 0; i < N; i++) copy[i] = original[i];
        }

void smallest_state(int* state, const int M, const int N)
{
        int i;

        for(i = 0; i < M; i++) state[i] = 1;

        for(i = M; i < N; i++) state[i] = 0;



}

int next_M_state(int* state, const int N)
```

```
{
int i = 0;

// Position der ersten 0 nach einer 1
int p = -1;
// Zahl der 1en bis zu dieser Position
int n = 0;

// beide Groessen bestimmen...
while(p == -1 && i < N)
        {
        if(state[i] == 1)
                {
                n++;
                }
        else
                {
                if(n > 0) p = i;
                }
        i++;
        }

// falls es eine 0 nach einer 1 gibt...
if(p != -1)
        {
        state[p] = 1;
        state[p-1] = 0;

        for(i = 0; i < n-1; i++) state[i] = 1;
        for(i = n-1; i < p-1; i++) state[i] = 0;

        return 1;
        }
// andernfalls...
else return -1;
```

```
        }

int dim_M(const int M, const int N)
        {
        // Zustand
        int state[N];

        smallest_state(state,M,N);

        // Dimension
        int dim = 1;

        // solange es weitere Zustaende gibt...
        while(next_M_state(state,N) == 1)
                {
                // ...Dimension erhoehen.
                dim += 1;
                }

        return dim;
        }

void gen_basis(int* states[], const int M, const int N, int dim)
{

        int state[N];

        smallest_state(state,M,N);
        for(int i = 0; i < N; i++) states[0][i] = state[i];
        for (int j=1; j<dim; j++)
        {

                next_M_state(state,N);
                for(int i = 0; i < N; i++) states[j][i] = state[i];
```

```
        }


}
```

To generate the Hamiltonian a sparse matrix is initialized and for a all possible combinations of elements of the above generated basis states it is checked whether the corresponding entry in the Hamiltonian is different from zero.

```
int zz_term(int* state, const int N)
        {
        int sum = 0;

        for(int i = 0; i < N/2-1; i++)
                {
                if(state[i] == state[i+1]) sum += 1; else sum -= 1;
                }

        for(int i = N/2; i < N-1; i++)
                {
                if(state[i] == state[i+1]) sum += 1; else sum -= 1;
                }
        return sum;
        }



int zz_term_cc(int* state, const int N)
        {
        int sum = 0;

        for(int i = 0; i <= N/2-1; i++)
                {
                if(state[i] == state[i+N/2]) sum += 1; else sum -= 1;
                }
```

```
        return sum;
        }



int xx_yy_term(int* state1, int* state2, const int N)
        {
        // aktuelle Position
        int i = 0;
        // Zahl der Fehler
        int errors = 0;
        // Position des 1. Fehlers
        int pos1 = 0;
        // Position des 2. Fehlers
        int pos2 = 0;

        // Fehler bestimmen
        while(i < N && errors < 3)
                {
                if(state1[i] != state2[i])
                        {
                        errors += 1;
                        if(errors == 1) pos1 = i;
                        else if(errors == 2) pos2 = i;
                        }
                i++;
                }

        // Fehler auswerten
        int coupled = 0;

        if(errors == 2 && state1[pos1] != state1[pos2])
                {
                if(pos2-pos1 == 1 && pos1!=N/2-1)
```

```
                {
                if(state1[pos1] == 1) coupled = 1; else coupled = -1;
                }

                }

        return coupled;
        }
```

```
int xx_yy_term_cc(int* state1, int* state2, const int N)
        {
        // aktuelle Position
        int i = 0;
        // Zahl der Fehler
        int errors = 0;
        // Position des 1. Fehlers
        int pos1 = 0;
        // Position des 2. Fehlers
        int pos2 = 0;

        // Fehler bestimmen
        while(i < N && errors < 3)
                {
                if(state1[i] != state2[i])
                        {
                        errors += 1;
                        if(errors == 1) pos1 = i;
                        else if(errors == 2) pos2 = i;
                        }
                i++;
                }
```

```
        // Fehler auswerten
        int coupled = 0;

        if(errors == 2 && state1[pos1] != state1[pos2])
                {
                if(pos2-pos1 == N/2)
                {
                if(state1[pos1] == 1) coupled = 1; else coupled = -1;
                }

                }

        return coupled;
        }



template <typename Matrix>
void init_Hamiltonian(const double J, const double Delta, const double Beta,
int* states[],Matrix& m, const int dim,const int N)
{

// Matrices are not initialized by default
    m= 0.0;

    // Create inserter for matrix m
    matrix::inserter<Matrix> ins(m);

// Zustaende
        int state1[N];
        int state2[N];

        // gekoppelte Zustaende
        int coupled;
```

```
        /*
        ****************************
        diagonale Elemente
        ****************************
        */
        //zz-Konstante innerhalb einer Kette
        const double prefactor_zz_term = J/4*Delta;
        //zz-Konstante zwischen den Ketten
        const double prefactor_zz_term_cc = prefactor_zz_term*Beta;

// diagonale Element druchlaufen...
        for(int i = 0; i < dim; i++)
                {
                // aktueller Zustand
                copy_state_from_into(states[i],state1,N);


// zz-Term der Heisenberg-Wechselwirkung
ins(i,i) = cdouble(zz_term(state1,N)*prefactor_zz_term+
zz_term_cc(state1,N)*prefactor_zz_term_cc,0);
                }

printf("Diagonalelemente erstellt\n");
/*
        ****************************
        nicht-diagonale Elemente
        ****************************
        */

        // Konstanten
        const double prefactor_xx_yy = J/2;
        const double prefactor_xx_yy_cc = Beta*J/2;

        for(int i = 0; i < dim; i++)
```

```
                {
                //printf("i=%d\n",i);
                for(int j = i; j < dim; j++)
                {
                // aktuelle Zustaende
                copy_state_from_into(states[i],state1,N);
                copy_state_from_into(states[j],state2,N);


                coupled = xx_yy_term(state1,state2,N);

                if(coupled != 0)
                {
                ins(i,j) += cdouble(prefactor_xx_yy,0);
                ins(j,i) += cdouble(prefactor_xx_yy,0);
                }


                coupled = xx_yy_term_cc(state1,state2,N);

                if(coupled != 0)
                {
                ins(i,j) += cdouble(prefactor_xx_yy_cc,0);
                ins(j,i) += cdouble(prefactor_xx_yy_cc,0);
                }

                }

                }

// Destructor of ins sets final state of m

}

 //Funktion: Bestimmt  Magnetisierungsschiefe
template <typename Matrix>
```

```
void init_magdiff(Matrix& m, int* states[], int dim, const int N)
{

                // Matrices are not initialized by default
                 m= 0.0;

                // Create inserter for matrix m
                matrix::inserter<Matrix> ins(m);
                int state[N];

                for (int j=0; j<dim; j++)
                {
                double sumlinks = 0;
                double sumrechts = 0;
                // aktueller Zustand
                copy_state_from_into(states[j],state,N);
                for (int i=0; i<=N/2-1; i++)
                {
                        if (state[i] == 1) sumlinks += 0.5;
                        else sumlinks -= 0.5;
                }
                for (int i=N/2; i<N; i++)
                {
                        if (state[i] == 1) sumrechts += 0.5;
                        else sumrechts -= 0.5;
                }
                ins(j,j) = cdouble(sumlinks - sumrechts,0);
                //printf("M(%d,%d)=%f\n",j,j,sumlinks-sumrechts);
                }



}
```

The energy shift in the Runge-Kutta scheme is calculated by 4 matrix vectors products with a shifted Hamiltonian.

```
 template <typename Matrix>
void init_eshift(Matrix& m, Matrix& H, int dim, double Ef)
{

                    // Matrices are not initialized by default
                     m= H;

                    // Create inserter for matrix m
                    matrix::inserter<Matrix> ins(m);

                    for (int i=0; i<dim; i++) ins(i,i)=H(i,i)-cdouble(Ef,0);




}

//Zufallsgenerator initialisieren
const gsl_rng_type * T;
       gsl_rng * r;



       gsl_rng_env_setup();

       T = gsl_rng_default;
       r = gsl_rng_alloc (T);

//Seed
gsl_rng_set(r,time(NULL));

//Magnetisierungschiefe initalisieren
compressed2D<cdouble>   Ma(dim, dim);
```

```
compressed2D<cdouble>    Maq(dim, dim);
compressed2D<cdouble>    Eshift(dim, dim);
compressed2D<cdouble>    Eshiftq(dim, dim);
compressed2D<cdouble>    Hq(dim, dim);
init_magdiff(Ma, states ,dim,N);
Maq=Ma*Ma;
Hq=Hamiltonian*Hamiltonian;

//Anfangszustand erstellen
dense_vector<cdouble>    state(dim, cdouble(0,0)),
v1(dim,cdouble(0,0)),v2(dim,cdouble(0,0)),
v3(dim,cdouble(0,0)),v4(dim,cdouble(0,0)),tmp(dim,cdouble(0,0));

for (int i=0; i<dim; i++)
{

state[i]=cdouble(gsl_ran_gaussian_ziggurat (r,1.0),
gsl_ran_gaussian_ziggurat (r,1.0));









}
tmp=state;

//Energieiteration ausfÃ¼hren
//Zielenergie eintragen
init_eshift(Eshift,Hamiltonian,dim,Ef);
Eshiftq=Eshift*Eshift;



double dte=0.01;
double temax=2;
int stepse = int (ceil(temax/dte));
```

```
for (int i=1; i<=stepse; i++)
{

        t=i*dte;
        v1=cdouble(-1,0)*dte*2*Eshiftq*state;
        v2=cdouble(-0.5,0)*dte*2*Eshiftq*v1;
        v3=cdouble(-1/3.0,0)*dte*2*Eshiftq*v2;
        v4=cdouble(-0.25,0)*dte*2*Eshiftq*v3;
        state += v1+v2+v3+v4;

}
```

Since the pure initial state is drawn at random from the unitary invariant emsemble a random number generator is needed. For this purpose the GNU Scientific Library (GSL) [61] is used. The above presented example for the Runge-Kutta energy filtering is only an excerpt from the original source code and not executable on its own. To iterate the state in real time the last few lines of code have to be changed to look like this

```
t=i*dt;
v1=cdouble(0,-1)*dt*Hamiltonian*state;
v2=cdouble(0,-0.5)*dt*Hamiltonian*v1;
v3=cdouble(0,-1/3.0)*dt*Hamiltonian*v2;
v4=cdouble(0,-0.25)*dt*Hamiltonian*v3;
state += v1+v2+v3+v4;
```

B. List of Publications

Steinigeweg, R. ; Niemeyer, H. ; Gemmer, J.: *Transport in the three-dimensional Anderson model: an analysis of the dynamics at scales below the localization length* In: *New Journal of Physics* 12 (2010), 113001.

Niemeyer, H. ; Schmidtke, D. ; Gemmer, J.: *Onset of Fokker-Planck dynamics within a closed finite spin system* In: *Europhys. Lett.* 101 (2013), 10011.

Khodja, A. ; Niemeyer, H. ; Gemmer, J.: *Transport in topologically disordered one-particle, tight-binding models* In: *Phys. Rev. E* 87 (2013), 052133.

Niemeyer, H. ; Michielsen, K. ; De Raedt, H. ; Gemmer, J.: *Macroscopically deterministic, Markovian thermalization in finite quantum spin systems* In: Submitted to Europhys. Lett.

Bibliography

[1] Uffinck, J. ; Butterfield, J. (Hrsg.) ; Earman, J. (Hrsg.): *Compendium to the foundation of statistical physics*. Amsterdam : Elsevier, 2007 (Handbook for the Philosophy of Physics). – 924–1074 S. 3

[2] Popescu, S. ; Short, A. ; Winter, A.: In: *Nature Physics* 2 (2006) 3, 4

[3] Beretta, G. P.: In: *J. Phys.: Conf. Ser.* 237 (2010), 012004 S. 3, 14

[4] Pauli, W.: *Über das H-Theorem vom Anwachsen der Entropie vom Standpunkt der Quantenmechanik*. Hirzel, 1928 (Probleme der Modernen Physik. Arnold Sommerfeld zum 60. Geburtstag, gewidmet von seinen Schülern) 4, 60

[5] Goldstein, S. ; Lebowitz, J. L. ; Tumulka, R. ; Zanghi, N.: In: *Eur. Phys. J. H* 35 (2010), NOV, Nr. 2, 173–200 S. `http://dx.doi.org/{10.1140/epjh/e2010-00007-7}`. – DOI 10.1140/epjh/e2010–00007–7 4

[6] Schroedinger, E.: *Statistical Thermodynamics*. Cambridge University Press, 1948 (A Course of Seminar Lectures) 4

[7] VanHove, L.: In: *Physica* 21 (1955), 517–540 S. 4

[8] Tasaki, H.: In: *Phys. Rev. Lett.* 80 (1998), 1373–1376 S. 4

[9] Page, D.N.: In: *Phys. Rev. Lett.* 71 (1993), 1291 S. 4

[10] Goldstein, S. ; Lebowitz, J. ; Tumulka, R. ; Zanghi, N.: In: *Phys. Rev. Lett.* 96 (2006), 050403 S. 4

[11] Gemmer, J. ; Mahler, G.: In: *Eur. Phys. J. B* 31 (2003), 249 S. 4, 49

[12] Reimann, P.: In: *Phys. Rev. Lett.* 99 (2007), 160404 S. 4, 27

[13] Reimann, P.: In: *Phys. Rev. Lett* 101 (2008), 190403 S. 4, 9, 12

[14] Linden, N. ; Popescu, S. ; Short, A. J. ; Winter, A.: Quantum mechanical evolution towards thermal equilibrium. In: *Phys. Rev. E* 79 (2009), Jun, S. 061103. http://dx.doi.org/10.1103/PhysRevE.79.061103. – DOI 10.1103/PhysRevE.79.061103 4

[15] RIera, A. ; Gogolin, C. ; Eisert, J.: In: *Phys. Rev. Lett.* 108 (2012), 080402 S. 4

[16] Deutsch, J. M.: In: *Phys. Rev. A* 43 (1991), 2046 S. 4, 14

[17] Srednicki, M.: In: *Phys. Rev. E* 50 (1994), 888 S. 4, 14

[18] Rigol, M. ; Dunjiko, V. ; Olshanii, M.: In: *Nature* 452 (2008), 854 S. 4, 14

[19] Dubey, S. ; Silvestri, L. ; Finn, J. ; Vinjanampathy, S. ; Jacobs, K.: In: *Phys. Rev. E* 85 (2012), 011141 S. 4

[20] Alicki, R. ; Lendi, K.: *Lecture Notes in Physics*. Bd. 286: *Quantum dynamical semigroups and applications*. Springer, 1987 4

[21] Caldeira, A. O. ; Leget, A. J.: In: *Physica A* 121 (1983), 587 S. 4, 15, 16

[22] Jin, F. ; De Raedt, H. ; Yuan, S. ; Katsnelson, M. I. ; Miyashita, S. ; Michielsen, K.: Approach to Equilibrium in Nano-scale Systems at Finite Temperature. In: *J. Phys. Soc. Jpn.* 79 (2010), S. 124005 4

[23] Trotzky, S. ; Chen, Y.A. ; Flesch, A. ; McCulloch, I.P. ; Schollwock, U. ; Eisert, J. ; Bloch, I.: In: *Nature Phys.* 8 (2012), 325–330 S. 4

[24] Tikhonenkov, I. ; Vardi, A. ; Anglin, J. R. ; Cohen, D.: In: *Phys. Rev. Lett.* 110 (2013), 050401 S. 4

[25] Ates, C. ; Garrahan, J. P. ; Lesanovsky, I.: In: *Phys. Rev. Lett.* 108 (2012), 110603 S. 4

[26] Ji, S ; Ates, C ; Garrahan, J P. ; Lesanovsky, I: In: *J. Stat. Mech.* 2013 (2013), P02005 S. 4

[27] Niemeyer, H. ; Schmidtke, D. ; Gemmer, J.: In: *Eur. Phys. Lett.* 101 (2013), 10010 S. 4, 21, 36, 38, 39, 40, 43, 45, 94, 95

[28] Khodja, A. ; Niemeyer, H. ; Gemmer, J.: In: *Phys. Rev. E* 87 (2013), 052133 S. 5

[29] Short, A.J.: In: *New Journal of Physics* 13 (2011), 053009 S. 9, 11, 12

[30] Reimann, P.: In: *New Journal of Physics* 12 (2010), 055027 S. 9

[31] Rigol, M.: In: *Phys. Rev. A* 80 (2009), 053607 S. 14

[32] Cassidy, A.C. ; Clark, C.W. ; Rigol, M.: In: *Phys. Rev. Lett.* 106 (2011), 140405 S. 14

[33] Beretta, G.P.: In: *Int. Journ. Quant. Inf.* 5 (2007), 249–255 S. 14, 15

[34] Ummethum, J.: *Transport in niedrigdimensionalen, wechselwirkenden Quantensystemen*, University of Osnabrueck, Diplomarbeit, 2008 20

[35] Moler, C. ; van Loan, C.: In: *SIAM Review* 45 (2003), 3 S. 21, 25

[36] Siek, J.G. ; Lumsdaine, A.: The Matrix Template Library: A Generic Programming Approach to High Performance Numerical Linear Algebra. In: *International Symposium on Computing in Object-Oriented Parallel Environments*, 1998 23

[37] Gottschling, P. ; Wise, D.S. ; Adams, M.D.: Representation-transparent matrix algorithms with scalable performance. In: *Proc. 21st Annual Int. Conf. on Supercomputing*, ACM Press, New York, 2007, S. 116 23, 71

[38] Abramowitz, M. ; Stegun, I.: *Handbook of Mathematical Functions*. Dover, New York, 1964 23

[39] Tal-Ezer, H. ; Kosloff, R.: In: *J. Chem. Phys.* 81 (1984), S. 3967 25

[40] Leforestier, C. ; Bisseling, R. H. ; Cerjan, C. ; Feit, M. D. ; Friesner, R. ; Guldberg, A. ; Hammerich, A. ; Jolicard, G. ; Karrlein, W. ; Meyer, H.-D. ; Lipkin, N. ; Roncero, O. ; Kosloff, R.: In: *J. Comp. Phys.* 94 (1991), S. 59 25

[41] Iitaka, T. ; Nomura, S. ; Hirayama, H. ; Zhao, X. ; Aoyagi, Y. ; Sugano, T.: In: *Phys. Rev. E* 56 (1997), 1222 S. 25

[42] Dobrovitski, V. V. ; De Raedt, H.: In: *Phys. Rev. E* 67 (2003), S. 056702 25

[43] De Raedt, K. ; Michielsen, K. ; Trieu, B. ; Arnold, G. ; Richter, M. ; Lippert, Th. ; Watanabe, H. ; Ito, N.: Massively parallel quantum computer simulator. In: *Comp. Phys. Comm.* 176 (2007), S. 121 – 136 25

[44] De Raedt, H. ; Michielsen, K.: Computational Methods for Simulating Quantum Computers . In: Rieth, M. (Hrsg.) ; Schommers, W. (Hrsg.): *Handbook of Theoretical and Computational Nanotechnology*. Los Angeles : American Scientific Publishers, 2006, S. 2 – 48 25

[45] Fehske, H. ; Schleede, J. ; Schubert, G. ; Wellein, G. ; Filinov, V.S. ; Bishop, A.R.: In: *Physics Letters A* 373 (2009), 2182 – 2188 S. 25

[46] Lebowitz, J. L.: In: *Physics Today* 46 (1993), 32 S. 26

[47] Lebowitz, J.L.: From Time-symmetric Microscopic Dynamics to Time-asymmetric Macroscopic Behavior: An Overview. In: *ArXiv e-prints* (2007), S. cond–mat/0709.0724 26

[48] Bartsch, C. ; Gemmer, J.: In: *Phys. Rev. Lett.* 102 (2009), 110403 S. 27

[49] Gemmer, J. ; Michel, M. ; Mahler, G.: *Quantum Thermodynamics*. Springer, Berlin, 2004 49

[50] Hove, L. van: In: *Physica* 23 (1957) 60

[51] Kreuzer, H. J.: *Nonequilibrium Thermodynamics and its Statistical Foundations*. Clarendon Press, 1981 60

[52] Joos, E.: *Das Verhalten quantenmechanischer Systeme unter ständiger Messung: Watchdog-Effekt und Master-Gleichung.*, Heidelberg, Diss., 1983 60

[53] Bartsch, C. ; Steinigeweg, R. ; Gemmer, J.: In: *Phys. Rev. E* 77 (2008) 60, 62, 96

[54] Dowker, H.F. ; Halliwell, J.J.: In: *Phys. Rev. D* 46 (1992) 60

[55] Paz, J.P. ; Zurek, W.H.: In: *Phys. Rev. D* 48 (1993) 60

[56] Joos, E. ; Zeh, H.D. ; Kiefer, C. ; Giulini, D. ; Kupsch, J. ; Stamatescu, I.-O.: *Decoherence and the Appearance of a Classical World in Quantum Theory.* Springer, 2003 60

[57] Griffith, R.: In: *J. Stat. Phys.* 36 (1984) 60

[58] Omnes, R.: In: *J. Stat. Phys.* 53 (1988) 60

[59] Gell-Mann, M. ; Hartle, J.B.: Addison Wesley, 1990 (Complexity, Entropy and the Physics of Information) 60

[60] Esposito, M. ; Gaspard, P.: In: *Phys. Rev. E* 68 (2003) 62

[61] Galassi, M. ; Davies, J. ; Theiler, J. ; Gough, B. ; Jungman, G. ; Alken, P. ; Booth, M. ; Rossi, F.: *GNU Scientific Library Reference Manual - Third Edition (v1.12).* Network Theory Ltd, 2009 83

List of Figures

List of Tables

Erklärung

Ich erkläre hiermit, dass ich diese Doktorarbeit selbständig verfasst, noch nicht anderweitig für andere Prüfungszwecke vorgelegt, keine anderen als die angegebenen Quellen und Hilfsmittel benutzt sowie wörtliche und sinngemäße Zitate als solche gekennzeichnet habe. Alle Rechnungen mit dem Chebyshev-Algorithmus sind in Kooperation mit dem Forschungszentrum Jülich entstanden.

Osnabrück, den 28. Oktober 2013